Copyright Warning & Restrictions

The copyright law of the United States (Title 17, United States Code) governs the making of photocopies or other reproductions of copyrighted material.

Under certain conditions specified in the law, libraries and archives are authorized to furnish a photocopy or other reproduction. One of these specified conditions is that the photocopy or reproduction is not to be "used for any purpose other than private study, scholarship, or research." If a, user makes a request for, or later uses, a photocopy or reproduction for purposes in excess of "fair use" that user may be liable for copyright infringement,

This institution reserves the right to refuse to accept a copying order if, in its judgment, fulfillment of the order would involve violation of copyright law.

Please Note: The author retains the copyright while the New Jersey Institute of Technology reserves the right to distribute this thesis or dissertation

Printing note: If you do not wish to print this page, then select "Pages from: first page # to: last page #" on the print dialog screen

ABSTRACT

POLARIMETRIC FIBER OPTIC WEIGH-IN-MOTION SENSOR

by
Jieping Wang

During the past decade, the demand for new methods of measuring the weight of moving vehicles has grown substantially. In the 1980's, several techniques for weighing vehicles in motion were developed. However, they often suffer from high installation and maintenance costs as well as low accuracy. This thesis describes a new technique based on polarization preserving optical fibers. A fibercore HB600 Bow-Tie fiber with an initial beat length of 1.16 mm was employed in the present study. Sensor response is discussed in terms of the effects of force amplitudes and velocities on the calibration parameter T_f. T_f is a function of the amplitude as well as the velocity of applied loading. Therefore, calibration of the sensor should be achieved through regression analysis of the load-fringe data for the entire spectrum of the desired force velocities. This also implied that the variation of beat length under such loading conditions is dependent on the amplitude and velocity.

POLARIMETRIC FIBER OPTIC WEIGH-IN-MOTION SENSOR

by
Jieping Wang

A Thesis
Submitted to the Faculty of
New Jersey Institute of Technology
in Partial Fulfillment of the Requirements for the Degree of
Master of Science in Electrical Engineering

Department of Electrical and Computer Engineering

October 1994

APPROVAL PAGE

POLARIMETRIC FIBER OPTIC WEIGH-IN-MOTION SENSOR

Jieping Wang

Dr. Farhad Ansari, Thesis Advisor — Date
Professor of Civil and Environmental Engineering, NJIT

Dr. Edip Niver, Committee Member — Date
Associate Professor of Electrical Engineering, NJIT

Dr. Haim Grebel, Committee Member — Date
Associate Professor of Electrical Engineering, NJIT

BIOGRAPHICAL SKETCH

Author: Jieping Wang

Degree: Master of Science in Electrical Engineering

Date: August 1994

Undergraduate and Graduate Education:

- Master of Science in Electrical Engineering
  New Jersey Institute of Technology
  Newark, NJ, 1994

- Master of Science in Computer Engineering
  Shanghai University of Technology
  Shanghai, P.R.China, 1991

- Bachelor of Science in Electrical Engineering
  Shanghai University of Technology
  Shanghai, P.R.China, 1985

Major: Electrical Engineering

This thesis is dedicated to
my parents, grandparents, and sister

ACKNOWLEDGMENT

The author wishes to express his sincere gratitude to his supervisor, Professor Farhad Ansari. His mastery of the subject matter combined with sincerity, enthusiasm, and encouragement, made this thesis a wonderful experience.

Many thanks are due to the distinguished members of my committee: Dr. Gerald Whitman and Dr. Edip Niver. Their suggestions and discussions have considerably improved the quality of the thesis.

The author also appreciates the timely help and suggestions from the Concrete Laboratory members: Been-jyh Yu, Rajendra Navalurkar, and Allyn Luke.

TABLE OF CONTENTS

TABLE OF CONTENTS
(Continued)

Chapter **Page**

LIST OF TABLES

LIST OF FIGURES

LIST OF FIGURES
(Continued)

Figure **Page**

CHAPTER 1

INTRODUCTION

1.1 Background and Objectives

Axle weights and axleweight distribution statistics for heavy vehicle traffic are required for the planning and management of programs for the maintenance, rehabilitation, upgrading and preservation of highways. Weight data can also be used for screening, identifying and removing potentially overweight vehicles and for monitoring the enforcement of license tax and load limit laws and regulations [15, 17].

For nearly 50 years, State highway agencies have routinely obtained this information through vehicle weight surveys consisting of static weighing techniques. These weight survey programs have required considerable expense to the agencies in terms of special site construction, personnel, and equipment. The owners and operators of vehicles selected for weighing have also been subjected to excess vehicles operating costs and time loss as a result of being diverted from the normal traffic stream to be stopped for weighing. As currently practiced, these weight surveys are often easily avoided by truck operators with overloaded vehicles, or by those who wish to avoid delays [20].

The need for more effective monitoring truck weight and vehicle type information has been shown by an analysis conducted by the FHWA Office of Highway Planning. In the analysis covering the 10 year period between 1969 and 1979, it was shown that while truck volumes had increased 25 percent on interstate rural highways, total equivalent single axle loading increased 153 percent. This was due to both an increase of total and percent trucks in the vehicle population and a shift in the truck population to larger, heavier trucks. These large trucks in 1969 continued 8 percent of the traffic stream on interstate rural highways; They now are 19 percent [10]. As a result of these increases, highway pavements are generally enduring their projected total lifetime equivalent singleaxle load applications in less than half that period. This analysis demonstrates that there is a critical need to upgrade and expand the activities of the States in monitoring truck characteristics.

Weigh-In-Motion (WIM) systems offer an alternative which avoids many of the problems identified above for static weighing systems. Types of WIM systems include: platforms in the pavement supported by load cells; bending plates and bridge deck systems using strain gauges; and lower cost, portable sensors which are affixed to the pavement surface.

Although most of these systems have produced satisfactory results, their usefulness has been limited by relatively high initial capital costs and operating

costs. This problem could be overcome by the successful development of a low-cost WIM system [10].

1.1.1 Objectives

Fiber optic sensors offer a number of advantages over the existing techniques among which are increased sensitivity, geometric versatility, in that fiber sensors can be configured in arbitrary shapes, they can be employed for sensing various physical perturbations such as acoustic, pressure, magnetic, temperature, rotation, and strain. More importantly, they can be employed under adverse environmental conditions where other types of sensors fail to operate.

The main objective for the work reported herein is to develop an understanding for the behavior of High-Birefringent optical fibers subjected to high amplitude dynamic compressive loads. This knowledge is fundamental for the design of weigh-in-motion sensors. The load can be considerably different (typically between 20 to 50 percent) from the static axle loads measured by a conventional weighbridge. Accurate determination of weights at different vehicle speeds require a sensor that it's signal output is independent of the frequency of applied loads. Shape linearity, and variations with frequency of the sensor signal have a direct bearing on the accuracy of weigh measurements. Conventional piezoelectric cables generate exponentially decaying output waveforms. In other words, the piezoelectric output signal peaks to a maximum value upon the

application of the load and decrease exponentially with time. On the other hand, fiber optic sensors are capable of maintaining linear response in relation to the applied load. Moreover, they are immune to the noise generated by electrical, temperature, and electromagnetic interference in the pressure transmission medium.

The frequency dependency of piezoelectric output signals implies that the variations in speed and axle spacing of vehicle produce large errors in the measured loads. Furthermore, piezoelectric sensors are more prone to damage, since their electronic components are in direct contact with the wheel. A key advantage in using optical cables as weigh measuring devices is the potential for real-time transmission of truck loading statistics via fiber optic telephone lines to a central computer to the local transportation authority, and therefore results in considerable cost savings in highway expenditures.

1.1.2 Literature Review and Product Search

The operating principles and instrumentation techniques employed in most portable WIM systems are straightforward. The implementation of these concepts, however, has required a relatively high degree of engineering skill and sophistication. The operating principles and features of the sensors incorporated in a variety of current portable WIM systems are described in the following sections.

Most of the existing portable WIM systems involve the monitoring and recording of output voltages which, in terms of magnitude, or magnitude and duration, are proportional to the wheel load. The output voltage are typically generated by the use of resistive, capacitive, or piezoelectric elements. Sensors described as oil filled mats or strips incorporate transducers which convert the change in fluid pressure into a measurable output voltage.

WIM system may conveniently be placed in one of the following categories:

- Where the whole vehicle activates the system.
- Where the system is successively activated by axle passages with all or half of the total wheel effective.
- Where the sensor is narrow and only part of the total wheel load activates the system.

An example of a system activated by a whole vehicle, category 1, is the currently marketed bridge WIM equipment where the strains produced in the loadbearing members of bridges by the passage of vehicles are sensed and used subsequently to obtain gross and distributed vehicle masses.

Most systems fall into category 2, in which the sensing element presents an area large enough to accommodate the wheels at one or both ends of the vehicle axles. Examples of such systems include:

- Metal deck with supporting load cells.

- Metal deck with integral strain gauges.
- Thin metal and rubber pad with integral strain gauges.
- Thin Metal and rubber pad constructed as a capacitor.
- Oil filled pad or mat.

(1) Capacitive System: The capacitive portable WIM system mentioned above is based on measuring the change in capacitance of two parallel horizontal plates when a load is imposed on the upper plate. The concept has been used to produce portable flexible weighing pads consisting of two or more parallel plates separated by a rubber flexible dielectric. Devices of this have been used in portable WIM systems in the United Kingdom, South Africa, and United States Arizona, Florida, and West Virginia [16-20].

The design for a flexible weighpad consisting of two or more parallel plates that act as the plates of a capacitor was first patented by Trott and Grainger in 1968. This sensor consisted of three perforated plates separated by and enclosed in layers of natural rubber. Subsequent inventions by others were devices of slightly different construction but which operated on the same principle. The most notable success with the capacitive weighpad device has been made by the National Institute for Transport and Road Research (NITRR) in South Africa [21]. The development and critical review of this system is briefly described in the following paragraphs.

The NITRR 3-plate capacitive sensor was described by Basson in 1977 [22]. Initial designs used steel mesh conductors separated by a polyurethane dielectric. Problems with the mechanical strength of the mesh and dielectric and the sensitivity of the polyurethane to changing loads led to a final design of steel plates separated by natural rubber and encased in a polychloroprene compound that had the required mechanical strength and was resistant to oil and water. The sensor unit measuring approximately 5.9 ft x 1.3 ft x 0.3 in (1.8m x 0.4m x 7mm) is secured to the road by means of perforated plates popriveted to its sides. The plates are fixed to the road with strips of bituminous tape and road nails. The sensor is placed in one wheel path and the axle loads are detected by roadside circuitry and accumulated in successive 4,400 lb. (2,000kg) bands, up to a maximum of 39,650 lb. (18,000 kg).

This equipment has had extensive testing in South Africa and has been the subject of more limited evaluation programs elsewhere. Results from South Africa indicate that the system gave accurate results assuming correct initial calibration for accumulated axle loading over large samples of vehicles. However, individual results are subject to large errors.

The NITRR axle load sensor is one of the few devices available which is truly portable since it does not require pavement excavation for its installation. Unfortunately, the high initial cost of the NITRR system and its inability to accurately determine individual axle loads has hampered its usefulness [23, 24].

In 1982, the Golden River Corporation began marketing a portable WIM system which incorporated the NITRR weight sensor with updated electronics [20]. The system consists of the axle weight sensor, a roadside unit, and a data retrieval device. The roadside unit scans the capacitive weighmat every milliseconds, producing a digital capacitance reading which is handled by signal processing algorithms. Axle counts in 12 user defined weight ranges are stored in solid state memory for selected time intervals of between 1 minute and 24 hours on the internal clock and calendar. Individual axle weights can also be displayed. Data retrieval is accomplished via a separate, microprocessor based device, or by telephone modem. Internal rechargeable batteries will support the retrieval units for several days and the roadside unit for about five weeks.

The performance of the system was tested in the United Kingdom and Arizona during November and December of 1982 [23]. Standard errors for individual axle weights were about +5 percent for heavy axles, corresponding to about 10 percent at 95 percent confidence. For medium axles, 95 percent confidence limits were about 15 percent. Some speed and temperature trends were evident, and subsequent software and hardware modifications were undertaken to compensate for these phenomena.

Road sensors for the Golden River Weighman classification and weighing unit include two inductive loops and one capacitive weighmat per lane. Vehicle classification is based on the number of axles, axle spacing and chassis height to

yield the 13 vehicle type categories specified in the FHWA's "F Series" classification scheme.

The Streeter Richardson Division of the Mangoon Corporation is also marketing a portable WIM system which includes the capacitive weighpad developed by NITRR [10,25,26]. The weight sensor is connected to a portable microcomputer with customized printed circuit boards. This portable WIM system is used with a gasoline powered generator.

Another portable axleweight sensor investigated in this research is the Swedish Weighpad developed by the Lund Institute of Technology [10]. This device is a 1/2 inch thick capacitive pad which can be nailed or screwed to the road surface. The pad consists of 7 elastic strips, each 13/4 inch wide, the capacitance of which changes with the passage of a wheel load. The capacitance change is converted to and analog voltage by dedicated electronic equipment. The pad has a row of lateral position sensors along one edge. It is said to measure load to an accuracy of +300 lb (136 kg), lateral placement to +4 inch (102mm), and passage times to +40 milliseconds, allowing the calculation of axle weights, vehicle placement, and vehicle speed. The device was regarded as research tool and has not been developed commercially.

(2) Piezoelectric Systems: Another axleweight sensor currently in use is the Vibracoax piezoelectric cable [27, 28]. The Vibracoax is a coaxial cable, 0.1 inch (3mm) in diameter, consisting of an inner copper conductor and an outer

copper sheath, separated by an insulator of compacted piezoelectric powder. The cable is produced in a variety of mountings by Thermocoat et cie of France and is commercially available through the Phillips Corporation and is available in an unmounted form or mounted in a rubber block with an extruded aluminum support [29].

Siffert reported in 1974 on work with Vibracoax sensors undertaken at Trappes Regional Laboratory (Paris West) [30, 31]. The French government has since conducted an extensive research, development, and implementation program using this technology. The general approach of these early field trials was to bury the unmounted Vibracoax in epoxy resin in a slot in the road surface. Vehicles with known axle weights were then driven over the installation and the piezoelectric sensor output was recorded. The results of these tests have not had wide circulation and have been available only as noted translations. They do, however, provide insight into the state of the art of this new technology as described below.

Siffert indicated that piezoelectric sensors were weather resistant and that optimum installation, depths were between 0.2 inch (6mm) and 0.4 inch (9mm). The signals were sufficiently clear so that axle counting was accurate to within +2 percent and speed measurements, using a U shaped piezoelectric sensor, were within 1 to 2 mi/h (2 to 3 km/h) of readings taken on a radar speedometer. Tests on the effect of speed on piezoelectric sensor signals indicated that the amplitudes of

raw signals were speed dependent, but that integration of the signals eliminated this trend. Work by Gloagan and Herbeuval [32] on the development of a dynamic axle weighing system indicated that the peak signal value, taken during an axle passage over the Vibracoax sensor was proportional not only to vehicle weight, but also to the foot print length of the tire. In addition, the signal amplitude was found to be approximately constant with vehicle speed, but was reduced by 30 to 40 percent if a vehicle decelerated or accelerated over the sensor. This effect was attributed to the increased contact area of the tire under these conditions. Comparisons of integrated piezo signals and static axle weights were reported to be within +10 percent, but only for a given speed. Integrated signals were proportional to weight and inversely proportional to speed. Additional research on the Vibracoax able indicated that speed measurements were within +8 percent to radar speed readings. Comparisons of vehicle weights with Vibracoax sensor outputs were conducted at three installations.

Results obtained from a sample of 75 weighed vehicles at one site where 9.8 ft (3m) sensors were used indicated that corrected dynamic weight recordings were within +20 percent of the static values 97 percent of the time. Vehicle speeds at this installation varied between 20 and 50 mi/h (32 and 80 km/h). The accurate calibration of each sensor was found to be critical in the determination of axle weights [31].

The Vibracoax cable has been used for some years as an axle sensor by Messdatd of Bornheim Hersel/Bonn, West Germany, and over 50 Vibracoax counters have been installed in that country. West Germany experience indicates that the charge produced by the sensor depends not only upon the axle load, but on pavement deformation which is, in turn, related to temperature, speed, and lateral position. United Kingdom experience with Vibracoax sensors has failed to produce accuracies comparable to those indicated in the French report.

1.1.3 Components of a Weigh-in-Motion System

There are several dimensions to the problems of vehicle classification and weigh in motion, including: the choice of weight sensor; its integration with other sensors to form an array for the measurement of speed, axle spacing, overall wheelbase, and vehicle class; sensor placement methods; microprocessor hardware and software; data storage; and data retrieval. Each of these various aspects is discussed below.

(1) Weight Sensors: The choice of weight sensor is the most fundamental aspect of the project. The emphasis of this research is on a portable, low cost system for which, to date, no wholly satisfactory weight transducer has been made commercially available. The main research and development activities of this effort will emphasize the production of a weight transducer capable of accounting for the axle forces the traffic flows imposed on the pavement.

Several categories of transducer are defined in the literature review. The main categories of transducer of interest in this study are:

- Capacitive systems, intended to measure load by monitoring a change in capacitance resulting from the mechanical deformation of a flexible dielectric. Piezoelectric transducers, which exhibit a property of certain natural and synthetic crystals, or in some cases, polymers whose molecular structure is such that an electrical charge is generated in response to dynamic stresses.
- Resistive system, which monitor the change in resistance of metals or other materials which are subjected to mechanical deformation due to the imposition of wheel loads.

It is believed that none of these approaches could provide a satisfactory accurate WIM sensor. The choice is then the introduction of a wholly new class of transducers for sensing the axle weights in a dynamic environment.

(2) Sensor Arrangement and Placement: Once weight and classification sensors have been selected, it is still necessary to decide upon the configuration into which they will be placed on the highway. The principle criterion in the selection of a suitable array is the ability to measure the vehicular parameters necessary for reliable and accurate classification of vehicle. There are several possible options which would satisfy the above requirement and these are described in detail in the section below in conjunction with a discussion of various methods of fixing the sensors into or onto the highway surface.

Vehicle classification can be based on the measurement of one or more of the following vehicular parameters: length, number of axles, wheelbase dimension(s), and sometimes a measure of the vehicle chassis height. However, the final choice of sensor for axle load determination will influence the type of sensor array that is adopted. It is essential to have at least one axle detector and it is anticipated that the weight will fulfill this role, thereby reducing the number of detectors required and total cost of the system. If the system is to be capable of detecting bicycles and motorcycles then, depending upon the sensitivity of the load measuring sensor, and extra axle detector may be necessary. For example, the capacitive weighmat system produced by Streeter Rechardson and Golden River is only capable of weighing individual axle loads over 600 lb.

(3) Microprocessor Hardware and Software: The preceding sections have described the development of traffic data collection techniques up to, and including, the advent of the microprocessor. Recent advances in this technology and the development of compact systems with high storage capacity have revolutionized all aspects of data collection. Traffic data acquisition using microprocessor based systems is now practical, enabling on-line monitoring of vehicle types and flows [33].

In 1978, Evans described the microprocessor as a programmable solid state device whose technology lies somewhere between the more conventional "hardware" solid state logic and the general purpose computer. The basic

microprocessor components are known as integrated circuits. A typical system includes a central processing unit to perform arithmetic and logical functions and to control data transfer between other system components or external data storage devices. The characteristics of these units that make them ideal for data collection and storage application are as follows:

- Capacity: large amounts of binarycoded data may be stored in very small units.
- Operational speed: manipulation of this data may be performed at high speed, enabling real-time monitoring of complex inputs.
- Compactness: complex microprocessor systems of high capacity may be housed in very small units.
- Power requirements: many systems require only a single 6 or 12 volts supply and consume very little current making them ideally suited for battery power.

(4) Data Retrieval and Storage: The way in which data are logged into the memory storage facility depends upon the number and type of variables that the user of the system wishes to gather. However, since there are a large number of potential users of the system, each with different requirements, it is necessary to determine the best format of collecting the data which would be of maximum benefit to all the parties concerned. Therefore, to ensure that the system could continue logging data for long periods of time without any retrieval of the data and without the memory becoming full, it is necessary to restrict the number of parameters that are stored.

1.2 Fiber Optic Sensors

Fiber Optic sensing techniques have been associated with precise and non-intrusive measurements. There are many advantages in using fiber optic sensors, such as good electrical isolation, immunity to electromagnetic interference, safety in explosive environments, compactness, and flexibility. Furthermore, fiber optic sensors exhibit high sensitivity.

In order to measure with high resolution a parameter such as the pressure, the Interferometric optical fibers sensors have been proposed during the past years. While the resolution is quite good, they present the disadvantage of a reference arm in which perturbations can occur. Such situations appear in the Mach-Zehnder interferometer. The polarimetric sensors use only one fiber with a strong linear birefringence, called hereafter the bias birefringence. The two arms of the interferometer become the two linear eigenstates of polarization, and the external stimulus like pressure modulates the phase difference between these two eigenstates, which has thus to be detected. It is essential in these sensors that the bias birefringence be strong enough to avoid any coupling between both eigenstates.

The fiber optic sensor used in this system belongs to the fiber optic polarimetric sensor. The optical fiber used in these sensors is highly birefringent(Hi-Bi). The polarimeter takes advantage of high-birefringence optical fiber to convert a stimulus from outside into a change in the state of polarization

(SOP). If anisotropy is introduced in the fiber, then the optical fiber can be constructed with dissimilar refractive indices along the X and Y axes. Hence, The velocities of the components of light transmitted along the two axes will be different and a phase difference is developed. Anisotropy can be achieved by building stress regions into fiber, as shown in the **bow-tie** birefringent fiber illustrated in Figure 1.1. Here, the slow axis is parallel to the high stress axis of the bow tie (parallel to the bow tie) and the fast axis is perpendicular to the high stress axis.

1.3 Matrix Representation of Polarization. The Jones Calculus

In the study reported here, circularly polarized monochromatic light was launched into a polarization maintaining fiber, and the output of light emitted from distal end of the fiber was studied as a function of dynamic compressive loads. Therefore, the theory and relationships describing polarization are given in this section.

1.3.1 Ways of Representing Light Waves

The electromagnetic radiation is predicted by Maxwell's theory to be a transverse wave motion. Associated with the wave are oscillating electric and magnetic fields that can be described with electric and magnetic vectors E and H and either of

them can be used to represent the light wave. In this thesis, the electric vector E has been employed for the representation of the light wave (Figure 1.2), defined as follows:

$$E = E_0 \cos(kz - wt) \tag{1.1}$$

where, E is the magnitude of light vector, E_0 is the amplitude of the wave, z is the position along the axis of propagation, k is called the wave number, w is the angular frequency. Here, k and w are further defined respectively as follows:

$$k = \frac{2\pi}{\lambda} \tag{1.2}$$

$$w = 2\pi \frac{c}{\lambda} \tag{1.3}$$

where, λ defined as the wavelength, c propagating velocity. For light in the free space, the propagating velocity is 30×10^8 m/sec.

It is often convenient to make use of the identity,

$$e^{i\theta} = \cos\theta + i\sin\theta \tag{1.4}$$

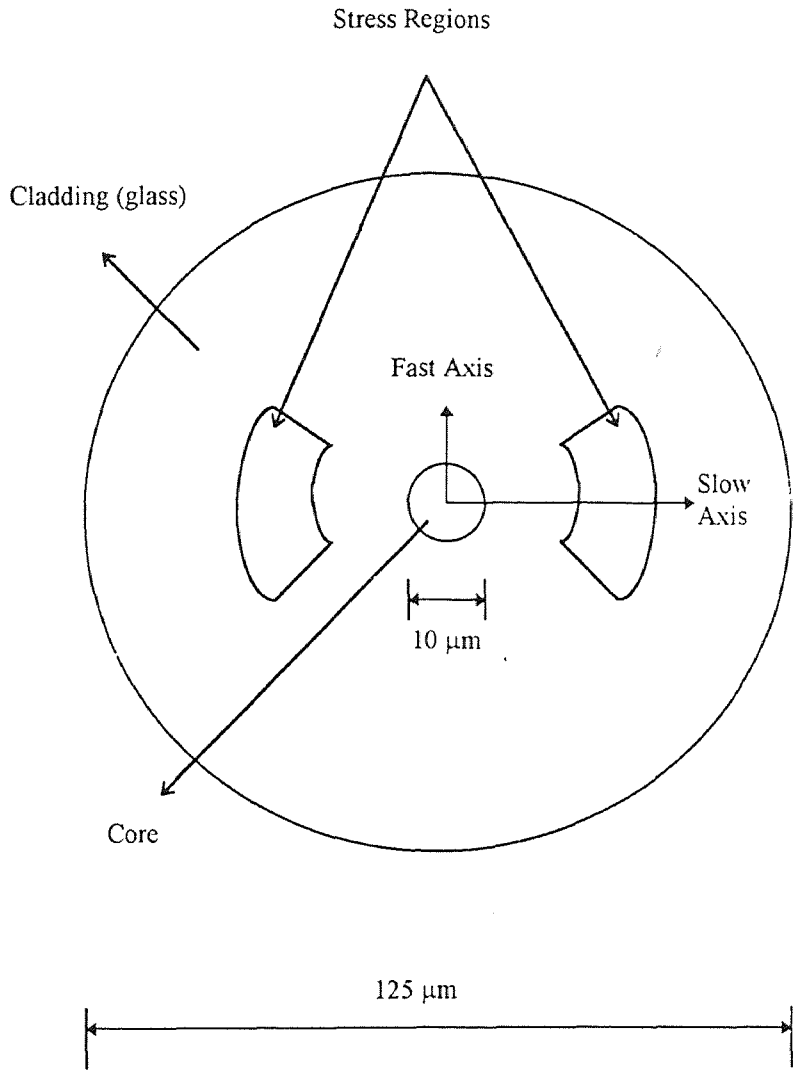

Figure 1.1 Cross section of a bow tie fiber

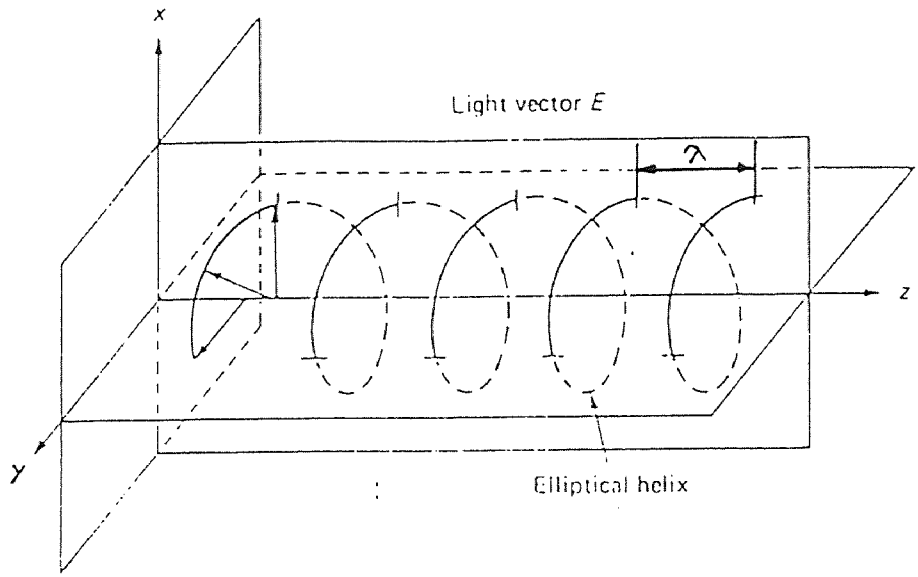

Figure 1.2 The elliptical polarized light vectors along the axis of propagation at a fixed instant of time

and write

$$E = E_0 e^{i(kz-wt)} \tag{1.5}$$

to represent the light wave in alternative way other than equation (1.1). It is understood that the real part is the actual physical quantity being represented. The real part is identical with the previous expression. The main reason for using the complex exponential expression is that it is algebraically simpler than the trigonometric expression.

1.3.2 Representation of Linear, Circular, and Elliptical Polarization

As we just explained in the preceding section, we can express the light wave by using exponential equation. It is sometimes convenient to employ a *complex vector amplitude* (ε_0) defined as follows:

$$\varepsilon_0 = \hat{x} E_0 + i \hat{y} E_0' \tag{1.6}$$

where, E_0 and E_0' represent different amplitudes of two linearly polarized waves polarized at right angles to each other along the x and y directions of a coordinate axes. Then the corresponding wave is

$$E = \varepsilon_0 \exp i(kz - wt) \tag{1.7}$$

This expression can represent any type of polarization. Thus if ε_0 is real, we have linear polarization, which the electric vector E maintains a constant orientation in space as follow along x direction in Figure 1.3:

$$E = \hat{x}E_0 \exp i(kz - wt) \tag{1.8}$$

If it is complex, we have elliptic polarization, which the electric field vector traces out an ellipse in space, as follow:

$$E = (\hat{x}E_0 + i\hat{y}E_0^{'}) \exp i(kz - wt) \tag{1.9}$$

In the special case of circular polarization, the real and imaginary parts of E are equal, which the electric field vector traces out an circle in space (Figure 1.4):

$$E = E_0(\hat{x} \pm i\hat{y}) \exp i(kz - wt) \tag{1.10}$$

and

$$E = E_0[\hat{x}\cos(kz - wt) + \hat{y}\sin(kz - wt)] \tag{1.10a}$$

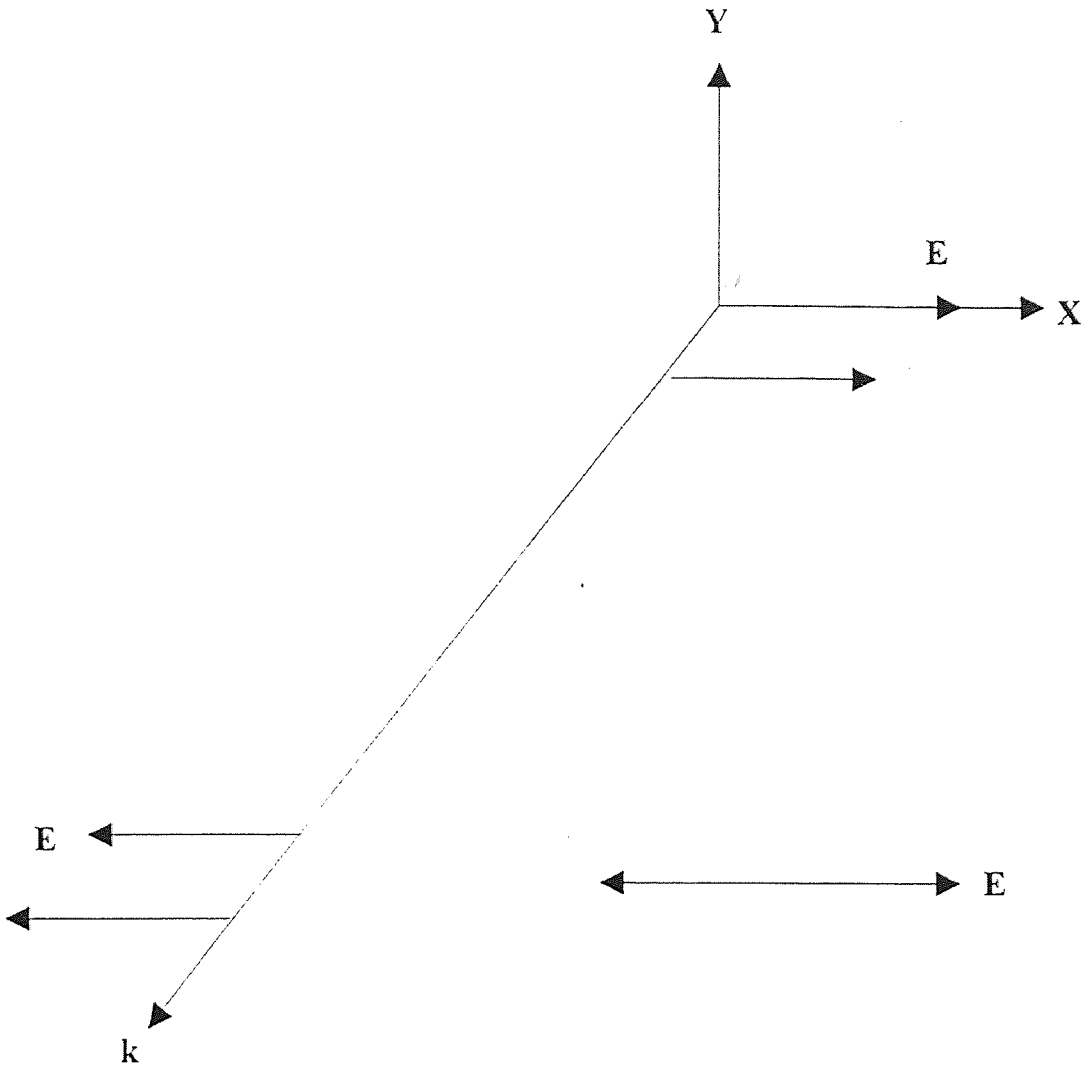

Figure 1.3 Fields in a plane wave, linearly polarized

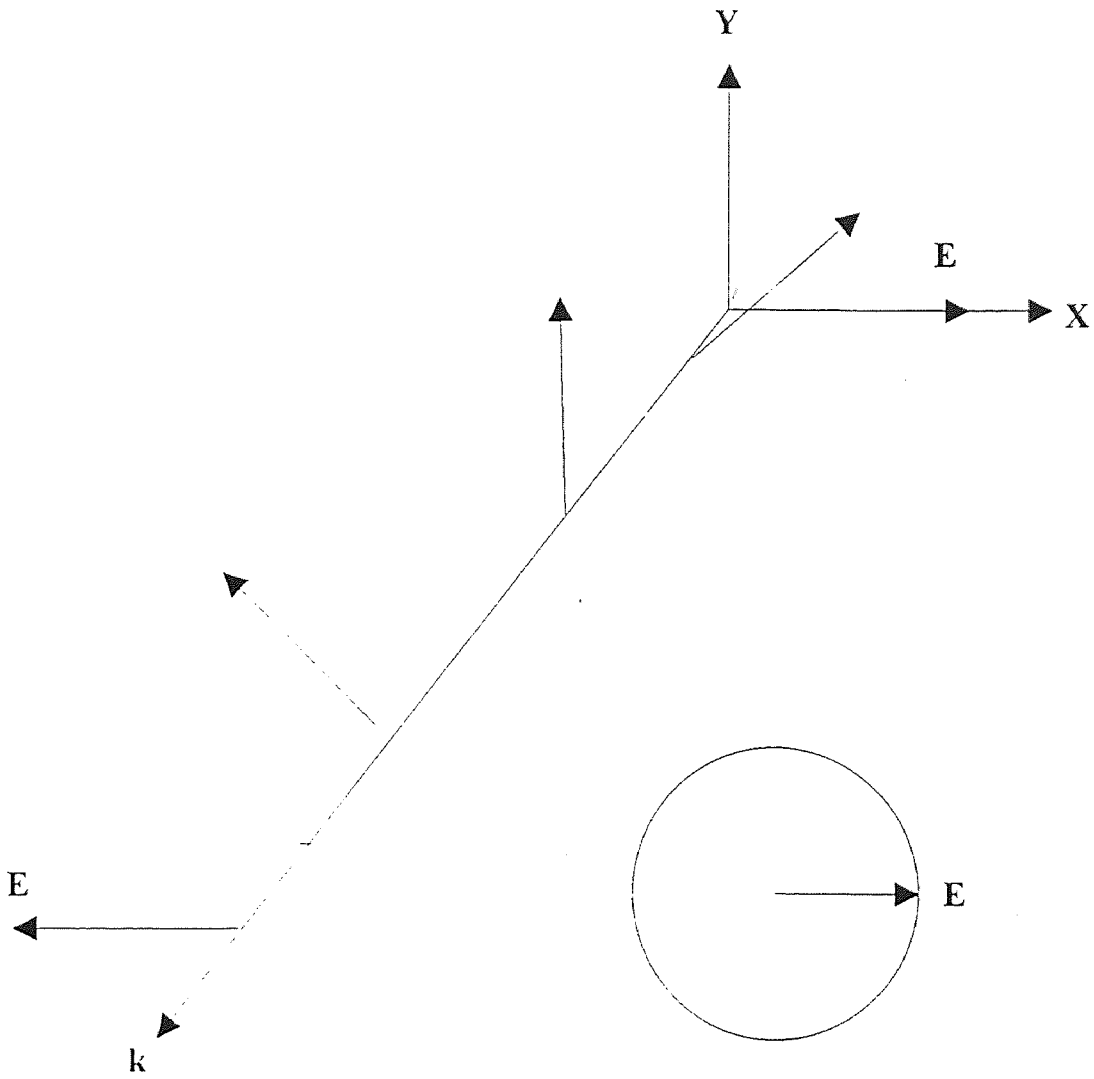

Figure 1.4 Fields in a circularly polarized wave

1.3.3 Jones Matrix Representation of Polarization

The complex vector amplitude given in the preceding section, equation (1.6), is not the most general expression because it was assumed that the x component was real and y component imaginary. A more general way of writing the complex amplitude of a light wave is

$$\varepsilon_0 = \hat{x}\,\varepsilon_{0x} + \hat{y}\,\varepsilon_{0y} \tag{1.11}$$

where ε_{0x} and ε_{0y} are both, possibly, complex. Accordingly, they can be expressed in exponential form as:

$$\varepsilon_{0x} = E_{0x}\, e^{i\phi_x} \tag{1.12}$$

$$\varepsilon_{0y} = E_{0y}\, e^{i\phi_y} \tag{1.13}$$

A convenient notation for the above pair of complex amplitudes is the following matrix known as the Jones vector [1]:

$$J = \begin{bmatrix} \varepsilon_{0x} \\ \varepsilon_{0y} \end{bmatrix} = \begin{bmatrix} E_{0x} e^{i\phi_x} \\ E_{0y} e^{i\phi_y} \end{bmatrix} \tag{1.14}$$

The normalized form of the Jones vector is obtained by dividing by the appropriate complex number such that the sum of the squares of the absolute values of the two components is unity. A useful, not necessarily normalized, form is obtained by division of whatever quantity results in the simplest expression. In this way, one can obtain a simple representation for the state of polarization of a light wave. For example, $\begin{bmatrix} 1 \\ 0 \end{bmatrix}$ represents a beam linearly polarized in the x direction, and $\begin{bmatrix} 0 \\ 1 \end{bmatrix}$ a beam linearly polarized in the y direction. The vector $\begin{bmatrix} 1/2 \\ 1/2 \end{bmatrix}$ or $\begin{bmatrix} 1 \\ 1 \end{bmatrix}$ represent a beam linearly polarized in a direction at 45 degree with respect to the x axis.

Another use of the matrix notation is that of computing the effect of inserting a linear optical element, or a train of such elements, into a beam of light of given polarization. The optical elements are represented by 2 x 2 matrices called *the Jones matrices*. The types of optical devices that can be so represented include linear polarizer, circular polarizers, wave plates, and so forth. Table 1.1 [6] are the matrices for several optical elements and fiber.

Any of the elements in Table 1.1 can be rotated with respect to some reference frame (usually the frame of the first element) using the standard rotation operation:

Table 1.1 Jones matrices for some linear optical elements

Optical Element	Polarization Orientation	Jones Matrix
Linear Polarizer	Transmission axis horizontal	$\begin{bmatrix} 1 & 0 \\ 0 & 0 \end{bmatrix}$
	Transmission axis vertical	$\begin{bmatrix} 0 & 0 \\ 0 & 1 \end{bmatrix}$
Quarter-Wave Plate	Fast axis horizontal	$\begin{bmatrix} i & 0 \\ 0 & 1 \end{bmatrix}$
	Fast axis vertical	$\begin{bmatrix} 1 & 0 \\ 0 & i \end{bmatrix}$
Half-Wave Plate		$\begin{bmatrix} -1 & 0 \\ 0 & 1 \end{bmatrix}$
Hi-Bi Fiber	$\phi \equiv \beta_{\Delta} L$ [1]	$\begin{bmatrix} e^{i\phi} & 0 \\ 0 & 1 \end{bmatrix}$

[1] ϕ is phase retardation of polarization fiber.
β_{Δ} is propagation constant
L is the length of fiber

$$[M(\theta)] \equiv [R^{-1}(\theta)][M][R(\theta)] \tag{1.15}$$

where, the rotation matrix, $[R(\theta)]$ is given by,

$$[R(\theta)] = \begin{bmatrix} \cos\theta & \sin\theta \\ -\sin\theta & \cos\theta \end{bmatrix} \tag{1.16}$$

In Table 1.1, we have two categories being considered: one is linear polarizer and another is quarter-wave plate, half-wave plate, and Hi-Bi fiber which all considered as linear retarders with phase retardation along two orthogonal polarization forms.

For linear polarizer, the general form of Jones matrix expression is as follow [6]:

$$J_{\text{polarizer}} = \begin{bmatrix} \cos^2\theta & \sin\theta\cos\theta \\ \sin\theta\cos\theta & \sin^2\theta \end{bmatrix} \tag{1.17}$$

where, θ is the angle of the eigenvector of linear polarizer to the x axis.

For linear retarder, the general form of Jones matrix expression is:

$$J_{retarder} = \begin{bmatrix} e^{i\phi}\cos^2\theta + \sin^2\theta & (e^{i\phi}-1)\sin\theta\cos\theta \\ (e^{i\phi}-1)\sin\theta\cos\theta & e^{i\phi}\sin^2\theta + \cos^2\theta \end{bmatrix} \quad (1.18)$$

where, ϕ is phase retardation between two orthogonal axes of linear retarder, whose fast axis subtends an angle θ with the x axis..

Thus, any of the matrix forms in Table 1 can be derived from either Eqn.. 1.17 or Eqn.. 1.18, depending on which category the optical element belongs to, by substituting the necessary parameters into θ and ϕ in equation, for example:

- For linear polarizer with transmission axis horizontal, we have $\theta = 0$, substituting into Eqn.. 1.17, we get as in Table 1:

$$J_p = \begin{bmatrix} \cos^2 0^0 & \sin 0^0 \cos 0^0 \\ \sin 0^0 \cos 0^0 & \sin^2 0^0 \end{bmatrix} = \begin{bmatrix} 1 & 0 \\ 0 & 0 \end{bmatrix} \quad (1.19)$$

- For quarter-wave plate, we know that its phase retardation $\phi = 90^0$, if now its fast axis makes an 0^0 angle with x axis (horizontal), then $\theta = 0^0$, substituting into Eqn.. 1.18, we get the matrix as in Table 1:

$$J_{quarter(0)} = \begin{bmatrix} e^{i90}\cos^2 0^0 + \sin^2 0^0 & (e^{i90}-1)\sin 0^0 \cos 0^0 \\ (e^{i90}-1)\sin 0^0 \cos 0^0 & e^{i90}\sin^2 0^0 + \cos^2 0^0 \end{bmatrix} = \begin{bmatrix} i & 0 \\ 0 & 1 \end{bmatrix} \quad (1.20)$$

- For Hi-Bi fiber, ϕ is phase retardation between its fast and slow axes, if now its fast axis makes an 0^0 angle with x axis (horizontal), then $\theta = 0^0$, substituting into Eqn.. 1.18, we get the matrix describing fiber as in Table 1:

$$J_{fiber} = \begin{bmatrix} e^{i\phi}\cos^2 0^0 + \sin^2 0^0 & (e^{i\phi} - 1)\sin 0^0 \cos 0^0 \\ (e^{i\phi} - 1)\sin 0^0 \cos 0^0 & e^{i\phi}\sin^2 0^0 + \cos^2 0^0 \end{bmatrix} = \begin{bmatrix} e^{i\phi} & 0 \\ 0 & 1 \end{bmatrix} \qquad (1.21)$$

Examples above are just three of matrices in Table 1.1, with the same procedure, we can get the rest of matrices in the table.

Finally, the Jones matrices are used as follows. Let the vector of the incident light be $\begin{bmatrix} A \\ B \end{bmatrix}$ or we can say $\mathbf{J}_{in}$ (Jones input) and the vector of the emerging light be $\begin{bmatrix} A' \\ B' \end{bmatrix}$ or $\mathbf{J}_{out}$ (Jones output). Then

$$\begin{bmatrix} a & b \\ c & d \end{bmatrix}\begin{bmatrix} A \\ B \end{bmatrix} = \begin{bmatrix} A' \\ B' \end{bmatrix}$$
$$[M]_{sys} J_{in} = J_{out} \qquad (1.21)$$

where $\begin{bmatrix} a & b \\ c & d \end{bmatrix}$ is the Jones matrix of the optical element. If light is sent through a train of optical elements, then the result is given by matrix multiplication:

$$\begin{bmatrix} a_n & c_n \\ b_n & d_n \end{bmatrix} \cdots \begin{bmatrix} a_2 & c_2 \\ b_2 & d_2 \end{bmatrix} \begin{bmatrix} a_1 & c_1 \\ b_1 & d_1 \end{bmatrix} \begin{bmatrix} A \\ B \end{bmatrix} = \begin{bmatrix} A' \\ B' \end{bmatrix}$$
$$[M_n] \ldots . [M_2][M_1] J_{in} = J_{out} \tag{1.22}$$

The matrix product above can be replaced by a *Jones system matrix* such that equation above becomes:

$$[M]_{sys} J_{in} = J_{out} \tag{1.23}$$

It should be noted that the Jones calculus is of use only for computing results with light that is initially polarized in some way. There is no Jones vector representation for unpolarized light.

CHAPTER 2

THEORETICAL BACKGROUND

2.1 The System Methodology

The optical arrangement shown in Figure 2.1 has been employed in this thesis. The light source is a He-Ne laser (30mW), where the emitted light is linearly polarized. The light emerging from the half-wave plate keeps the light linearly polarized without any significant change in the amplitude of light emitting from the laser. The angle of polarization can be easily changed as needed by rotating the half-wave plate through desired angles. To produce circularly polarized light, a quarter-wave plate is positioned at an angle of 45 degrees with respect to the linearly polarized light. The circularly polarized light is launched into the fiber and excites the two orthogonal principal directions equally. Then the light emitted from the optical fiber is send through a quarter-wave plate which is positioned at an angle of -45 degrees with respect to the x axis, and analyzed by a polarizer positioned in an angle of 0 degrees with respect to the x axis.

The propagation of polarized light within the sensor system in Figure 2.1 can be described by Jones calculus as explained in Chapter 1 where it is assumed that the optical fiber can be identified as a retarder.

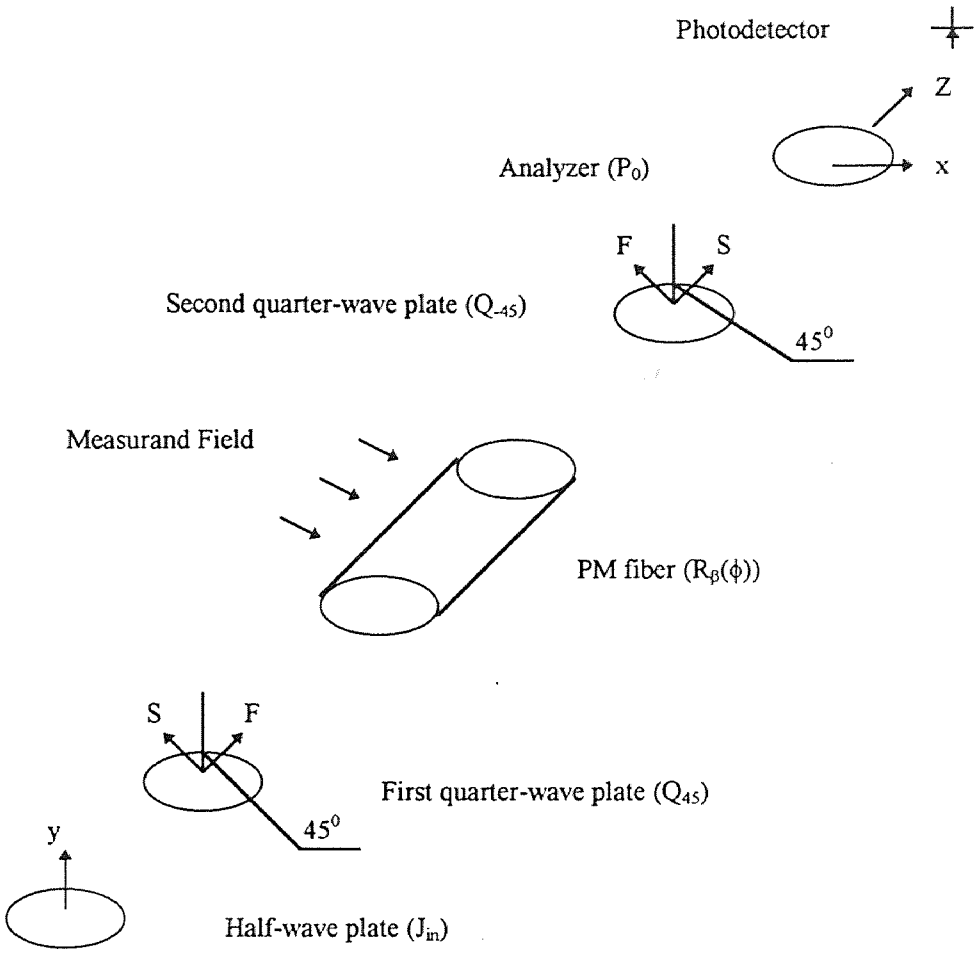

Figure 2.1 Typical optical arrangement for a fiber optic polarimetric sensor

The Jones matrix description of this system (in Fig. 2.1) is as follows:

$$J_{out} = P_0\, Q_{-45}\, R_\beta(\phi)\, Q_{45}\, J_{in} \qquad (2.1)$$

where, J_{in} stands for half wave plate considered as linear polarizer, whose optical axis is vertical.

Q_{45} for first quarter-wave plate, whose fast axis makes an angle 45^0 with the x axis

$R_\beta(\phi)$ for Hi-Bi fiber with phase retardation ϕ, whose fast axis makes an angle β with the x axis.

Q_{-45} for second quarter-wave plate, whose fast axis makes an angle -45^0 with the x axis.

P_0 for analyzer, whose optical axis is horizontal.

and the system frame is aligned with the horizontal axis (x axis).

Here, the output of half wave plate functions the same way as a linear polarizer. By using a half wave plate, it is possible to change the direction of the linearly polarized light without any loss in amplitude. Therefore, it can give us much more flexibility of changing the angle of linear polarized light while keeping amplitude of that light.

The Jones matrix for the quarter-wave plate, whose fast axis makes an angle $\pm 45^0$ with the x axis (horizontal), are obtained from Eqn. 1.18 by substituting 90^0 for ϕ and $\pm 45^0$ for θ. Thus, we obtain either Q_{45} or Q_{-45} for $\theta = 45^0$ or $\theta = -45^0$ respectively:

$$Q_{45} = \frac{1}{2}\begin{bmatrix} i+1 & i-1 \\ i-1 & i+1 \end{bmatrix} = \frac{i+1}{2}\begin{bmatrix} 1 & i \\ i & 1 \end{bmatrix}$$
$$Q_{-45} = \frac{1}{2}\begin{bmatrix} i+1 & 1-i \\ 1-i & i+1 \end{bmatrix} = \frac{i+1}{2}\begin{bmatrix} 1 & -i \\ -i & 1 \end{bmatrix} \quad (2.2)$$

J_{in} and P_0 can also be represented in matrix form through Table 1.1 as:

$$J_{in} = \begin{bmatrix} 0 \\ 1 \end{bmatrix}$$
$$P_0 = \begin{bmatrix} 1 & 0 \\ 0 & 0 \end{bmatrix} \quad (2.3)$$

Then, by taking into account Eqn. 1.18 for Hi-Bi with fast axis oriented β degrees with respect to the horizontal (θ = β), we obtain:

$$J_{out} = \begin{bmatrix} 1 & 0 \\ 0 & 0 \end{bmatrix}\frac{i+1}{2}\begin{bmatrix} 1 & -i \\ -i & 1 \end{bmatrix}\begin{bmatrix} e^{i\phi}\cos^2\beta + \sin^2\beta & (e^{i\phi}-1)\sin\beta\cos\beta \\ (e^{i\phi}-1)\sin\beta\cos\beta & e^{i\phi}\sin^2\beta + \cos^2\beta \end{bmatrix} \times \left(\frac{i+1}{2}\right)\begin{bmatrix} 1 & i \\ i & 1 \end{bmatrix}\begin{bmatrix} 0 \\ 1 \end{bmatrix} \quad (2.4)$$

After simplifications, Eqn 2.4 can be reduced to

$$J_{out} = \frac{1}{2}\begin{bmatrix} (1-e^{i\phi})e^{-i2\beta} \\ 0 \end{bmatrix} \quad (2.5)$$

The intensity of the emerging light from the analyzer expressed by Eqn. 2.5 is:

$$I = \tilde{J}_{out} J_{out} = \frac{1}{4} e^{i2\beta} \begin{bmatrix} 1 - e^{-i\phi} & 0 \end{bmatrix} e^{-i2\beta} \begin{bmatrix} 1 - e^{i\phi} \\ 0 \end{bmatrix} = \sin^2 \frac{\phi}{2} \qquad (2.6)$$

Inspection of Eqs. 2.6 indicates that the intensity of light beam emerging from the system is a function only of ϕ (the phase retardation inside fiber sensor) since β, the angle of fast axis with respect to the system frame (x axis) do not appear in the amplitude of the wave.

2.2 Relationship Between the Fiber Signal and Applied Load

As we have already seen from Eqs. 2.6, there is a direct sine wave relationship between intensity of light wave emerging from the analyzer of a circular polariscope (Figure 2.1) and relative retardation ϕ between the two perpendicular components of the polarized light in Hi-Bi fiber. This relative phase retardation in a Hi-Bi fiber of a length L_0 can be expressed as:

$$\phi = \phi_x - \phi_y = \frac{2\pi L_0}{\lambda} (n_x - n_y) \qquad (2.7)$$

where, n_x-n_y is the different between the effective indices of the polarization modes and

$$B = n_x - n_y \tag{2.8}$$

is the birefringence,

$$\beta = \frac{2\pi}{\lambda} B \tag{2.9}$$

is denoted as propagation constant where λ is the wavelength of the light wave.

The actual condition inside the fiber is one of multiple polarization states, with two consecutive points of equal phase being a beat length apart from each other, where the beat length, L_B is defined as:

$$L_B = \frac{2\pi}{\beta} \tag{2.10}$$

From Eqs. (2.7) and Eqn. (2.9), we can get,

$$\phi = \beta L_0 \tag{2.11}$$

Bock, et. al. [4] developed the relationship describing the variation in beat length due to hydrostatic pressure. Our formulation follows the analysis given in [4]. However, in present study's case instead of pressure the sensor is subjected to a compressive load, and therefore, we define f to be the applied force per unit length, or the force intensity on the fiber, then

$$f = \frac{F}{L} \tag{2.12}$$

where, F is the force applied by the servo-hydraulic testing machine, and L is the length of optical fiber under load. The force intensity, f modulates the relative phase retardation, ϕ which already exists between the two axes of the Hi-BI fiber, according to the following relationship:

$$\frac{\partial \phi}{\partial f} = \frac{\partial \beta}{\partial f} L + \frac{\partial L}{\partial f} \beta \tag{2.13}$$

The modules of compression for silica, K, which is the ratio of compressive stress to cubical compression is measured in [5] and it is equal to $0.377*10^{12}$ d/cm^2 This translates into less than a fraction of one percent for the range of compressive loads employed in this thesis. Therefore, the effect of compressive load on length of the fiber can be ignored, and Eqn. (2.13) can be reduced to:

$$\frac{\partial \phi}{\partial f} = \frac{\partial \beta}{\partial f} L_0 \tag{2.14}$$

From the relation in Eqn.(2.9) and equation above, we can get

$$\frac{\partial \beta}{\partial f} = \frac{2\pi}{\lambda} \frac{\partial B}{\partial f} \tag{2.15}$$

Thus, combining Eqs.(2.14) and (2.15), we arrive at,

$$\frac{\partial \phi}{\partial f} = \frac{2\pi L_0}{\lambda} \frac{\partial B}{\partial f} \tag{2.16}$$

As we already defined the beatlength in Eqn.(2.10) and relation in Eqn. (2.9), we have another relation,

$$B = \frac{\lambda}{L_B} \tag{2.17}$$

From that, we can have,

$$\frac{\partial B}{\partial f} = \lambda \frac{\partial}{\partial f} \left(\frac{1}{L_B}\right) \tag{2.18}$$

or

$$\frac{\partial \phi}{\partial f} = 2\pi L_0 \frac{\partial}{\partial f}\left(\frac{1}{L_B}\right) \tag{2.19}$$

Providing the length of the fiber without external force is equal to a multiple of the beat length,

$$L_0 = nL_{B_0} \tag{2.20}$$

where, L_{B_0} is the beatlength at f=0, and n is a multiple which does not have to be an integer, assuming a decrease of the beat length parameter at applied load f, then the change in beat length under load can be represented as follows:

$$L_0 = L_B(n+k) \tag{2.21}$$

where k is an integer representing additional k-values of beat length which are suppressed within the same distance L_0 of the fiber, since the fiber length remains fixed. L_{B_0} and L_B are beat lengths without external force and under force, respectively.

By eliminating n from Eqs. (2.20) and (2.21), we arrive at,

$$L_0 = L_B\left(\frac{L_0 + kL_{B_0}}{L_{B_0}}\right) \tag{2.22}$$

To rearrange terms in above equation, we have,

$$\frac{1}{L_B} = \frac{1}{L_{B_0}} + \frac{k}{L_0} \tag{2.23}$$

Hence, the change in beat length as a function of compressive load intensity can be as:

$$\frac{1}{L_B} = \frac{1}{L_{B_0}} + \frac{f}{L_0 T_f} \tag{2.24}$$

where, T_f is defined as the amount of unit force f to induce a 2π phase shift of a polarized light and can be determined experimentally by measuring the output fringe as a function of f as shown in Figure 2.2. It is related to k by

$$T_f = \frac{f}{k} \tag{2.25}$$

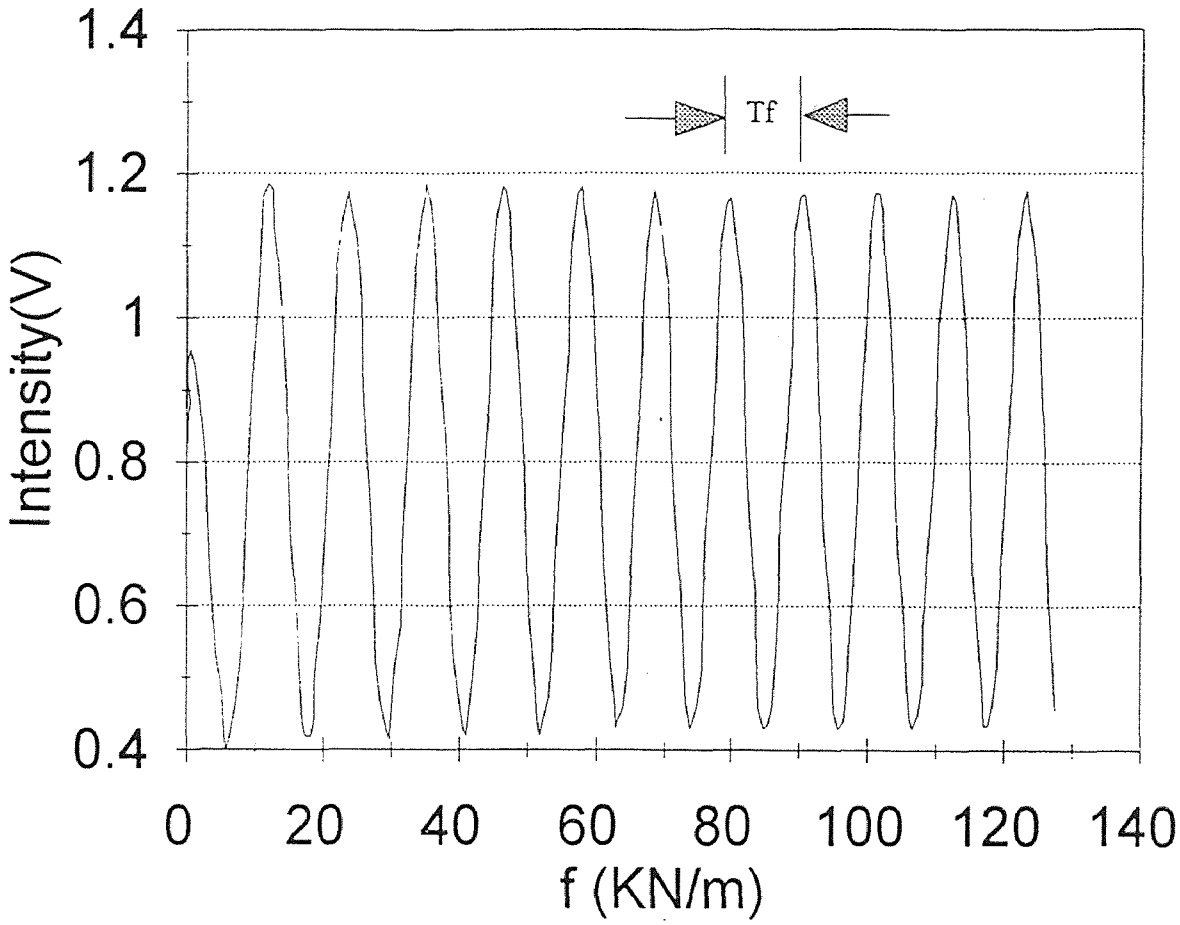

Figure 2.2 T_f defined as 2π phase shift on amount of unit force

As shown in Eqn. (2.24), T_f is proportional to the rate of change of beat length with respect to the applied unit force, and it can be employed as a calibration factor for the computation of loads, provided that its magnitude is independent of the velocity of loading. Our experimental results have indicated that for sensors subjected to high amplitudes of dynamic compressive force, T_f varies both with the amplitude and the velocity of applied loading. Therefore, these effects need to be incorporated into Eqn. (2.24).

CHAPTER 3

EXPERIMENTAL STRUCTURE AND PROGRAM

The experimental setup consisting of the polarizing optics and the servo-hydraulic loading system are depicted in Figure 3.1. Circularly polarized monochromatic light was launched into a Fibercore HB600 Bow Tie fiber. A 30 mW polarized Helium-Neon laser operating at 632.8 nm was employed as the light source. The relatively high output power of the laser eliminated the need for signal modulation. The light at the output end of the PM fiber was launched into a detector-amplifier assembly and the data was subsequently fed into a data acquisition device for computer processing and data analysis.

3.1 MTS Testing Machine

The loading element employed in this thesis for the application of dynamic load to the fiber sensor consisted of a stiff frame, closed-loop servo-hydrostatic testing machine manufactured by MTS System Corporation and capable of applying up to 445 KN of tensile or compressive load.

The MTS testing machine includes three major parts: Model 458.20 MicroConsole™, The Model 458.11 DC Controller, and the Model 458.90

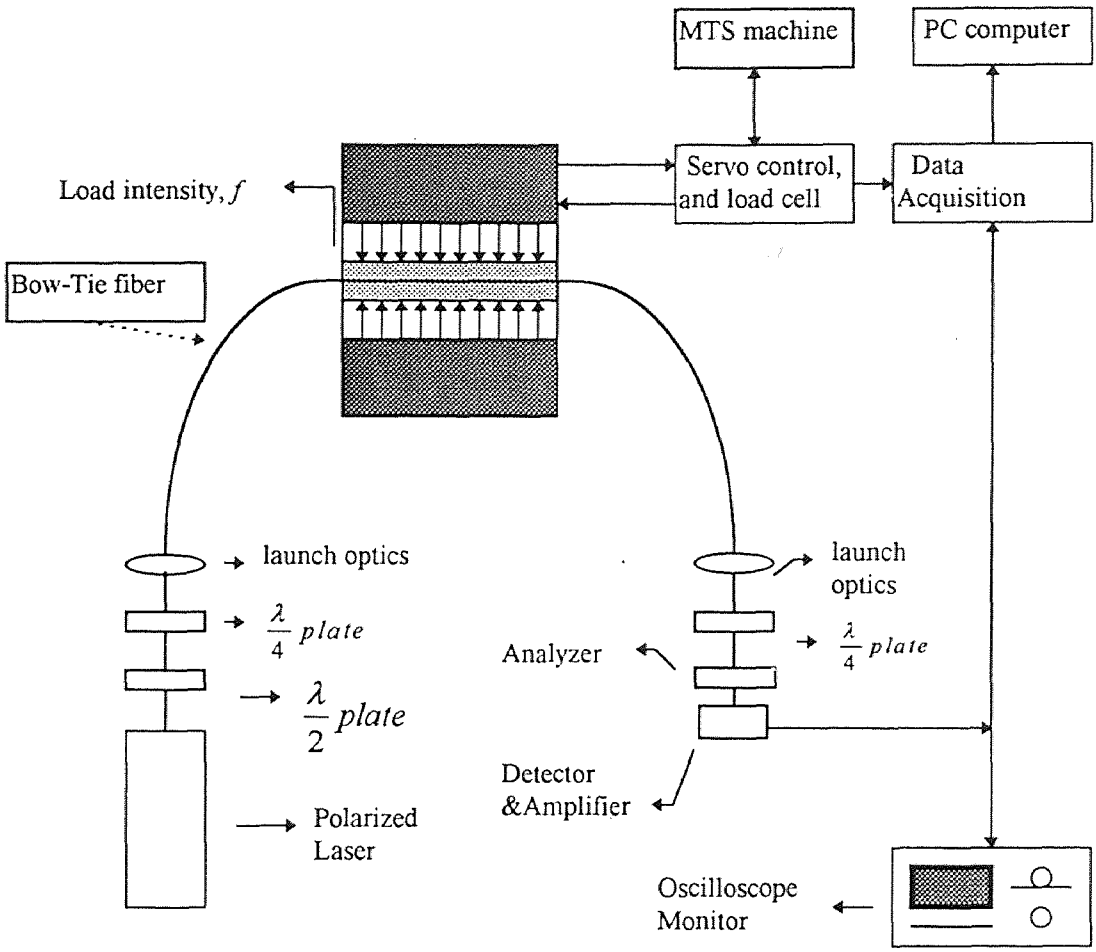

Figure 3.1 Experimental setup for dynamic loading of Hi Bi sensor

Function Generator and each of them has special function contributing to the loading program in this study. The various components of the MTS system are described as follow:

- The Model 458.20 Microconsole, which located in the front panel, provides a multifunction digital display, cycle counter, program and record control, hydraulic pressure control, and an internal power supply for the plug-in modules, it is a main part of the whole controlling system.
- The Model 458.11 DC Controller is a plug-in module used in the MicroConsole to provide: transducer conditioning as to the magnitude of desired load or deformation, command conditioning, servovalue control, and error detection and limit detection. Its operating controls and indicators are located on the DC Controller front panel and the MicroConsole front panel. Input and output connections are made at MicroConsole rear panel connection. It is this part that decides how much load intensity you want to apply on the specimen, and also together with previous model, to get feed back control.
- The model 458.90 Function Generator is also a plug-in module used in the Model 458 MicroConsole to provide the internal dynamic program command to the servo control loop. Its output waveform may be selected for square or ramp waveform to accommodate actual loading pattern. The output frequency may be adjusted to fit for the frequency of the dynamic load or different loading rate. Also, its operating controls and indicators for the function

generator are located on both the function generator front panel and the MicroConsole front panel.

For dynamic loading application, the loading capacity decrease as a function of applied loading velocities. This is due to the limitations associated with the hydraulic pump capacity.

3.2 Optical Source and System

The optical source is a 632.8 nm STABILITE^{TM} He-Ne laser manufactured by Spectra-Physics company. It is a powerful (30 mW) and pre-polarized laser which provides a stable laser light. The optical system consisted of a half wave plate, one plane-polarizer, two quarter wave plates, and two bare fiber (FC) adapters for connecting the polarization-maintaining (PM) fiber to the optical and electronic assembly.

The light from He-Ne laser was first coupled into the half-wave plate and then into the first quarter wave plate. The axes of the half wave plate and the quarter wave plate were set at 45^{o} with respect to each other. The PM fiber was connected to the quarter wave plate via the FC fiber adapter.

The bow-tie high birefringence optical fiber (HB600) manufactured by Fibercore LTD was employed in this project. The bow-tie fiber which operates at a wavelength of 630 nm has a cladding diameter of 125 um, coating diameter of 250 um, and a maximum attenuation 12 dB/km.

At the receive end of the system, the fiber adapter was connected to the second quarter wave plate from which the output light was passed through the analyzer. The axes of the second quarter wave plate and the analyzer were set at 45^{o} with respect to each other.

The optical signal emerging from the optical system propagates into the photo-detector. There, the optical signal which here indicates the amplitude of light is converted into the electrical signal and then amplified by the analog amplifier. The photo detector and the amplifier assembly are shown in Figure 3.2. the photo detector (AXGS-R2F) is manufactured by SHARP. Data which carried required information from the amplifier were then transferred via data acquisition board to the PC computer to process.

3.3 Data Acquisition

A data acquisition board with an analog to digital converter is employed for the transfer and storage of data into IBM PC/AT/286 computer. DAS-20 A/D & D/A data acquisition board manufactured by KEITHLEY METRABYTE CORP. is a multifunction, high-speed, 8 channel/16 channel, I/O expansion board that turns a host computer into a precision data-acquisition and signal-analysis instrument. The board plugs directly into any expansion slot of IBM PC /AT, or compatibles. The full scale input of each channel is ±10 volts. A/D conversion time is typically 8.5 μs. The description of the structure and the programming details of this board are

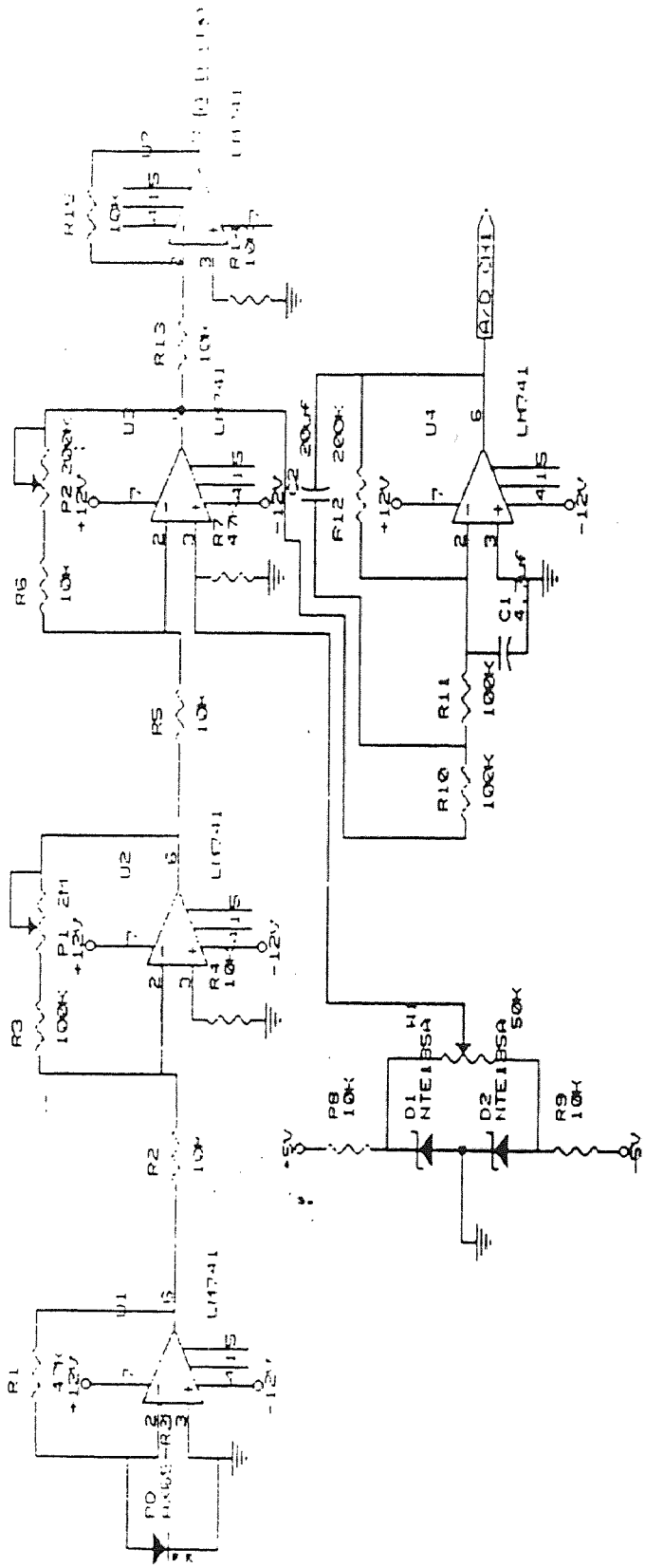

Figure 3.2 Photo detector and amplifier

shown in [3]. The output of the analog amplifier is connected to the input of data acquisition board Channel 7, along with load cell signal to channel 1. So two separate channels of data plus time are recorded simultaneously when the system is in operation. To simulate truck loading at various speeds, the fiber optic sensor was loaded at different speeds and frequencies. To capture all the information, data acquisition rate was varied from 1 to 300 Hz for slow and fast rates of loading respectively.

All the experiments were recorded through DAS-20 data acquisition board and the process is controlled by LABTECH NOTEBOOK software of Laboratory Technologies Corporation. Several NOTEBOOK parameters which needed to be set prior to the commencement of test were:

- Number of Channels: 2 (Chan. 1 for Load, 7 for fiber signal) + time channel
- Sampling Rate, Hz: 1 ~ 300
- Buffer Size: 10000
- Run Duration, sec: 1000
- Columns in Each File for Data: 3 (1st for time, 2nd load, 3rd fiber)

3.4 Specimen Preparation

The structure and geometry of the specimen employed in this thesis is depicted in Figure 3.3. In the current configuration, the 250 micron thick fiber was

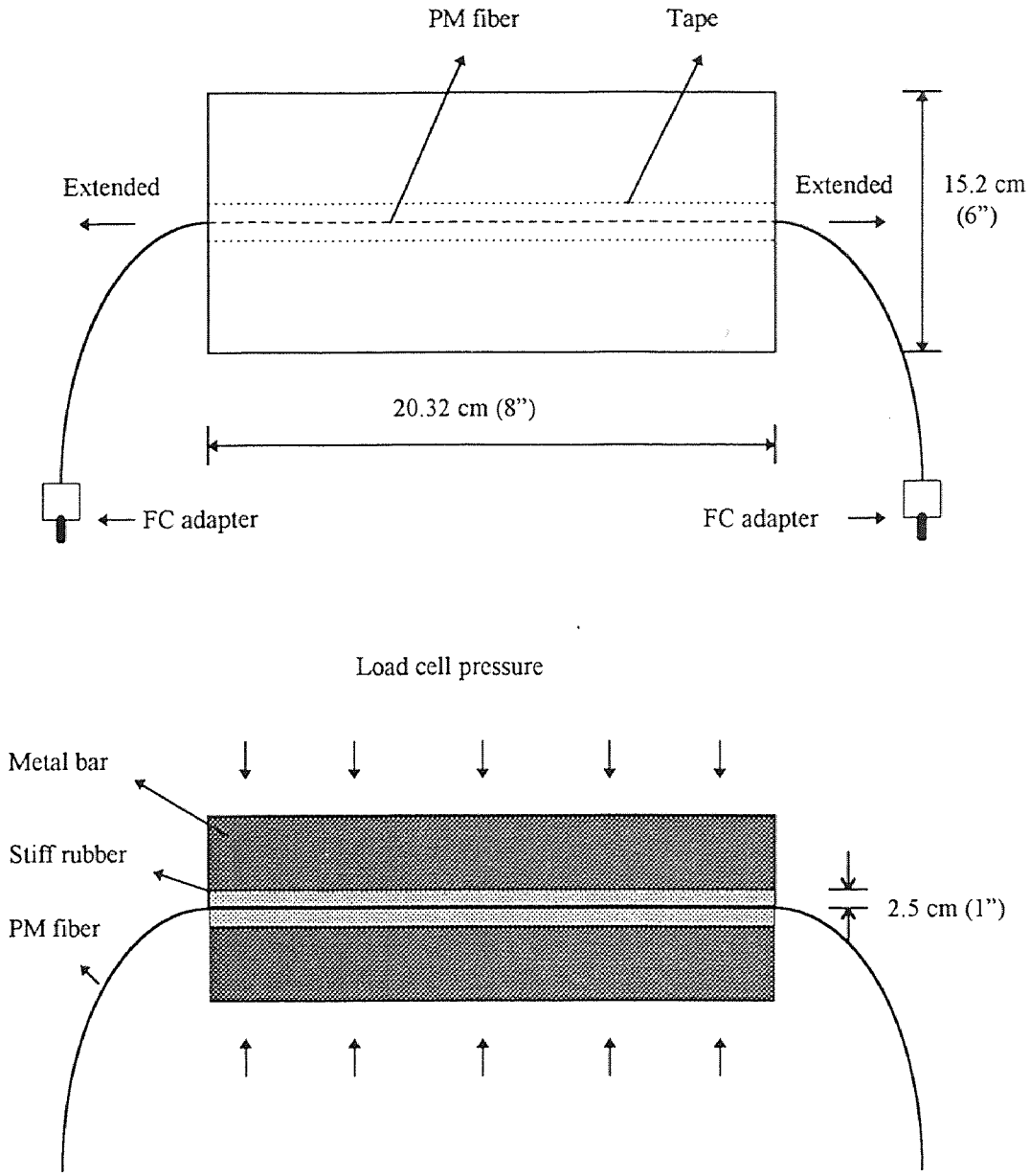

Figure 3.3 Specimen geometry

sandwiched between two 2.5 cm thick stiff rubber pads. Rubber pads provided protection against damage by the applied loads. For the configuration shown in Figure 3.3, the fiber is fully extended in a straight line and taped to one of the rubber pads. Fiber ends were cleaved flat and were subsequently connected to the optical system via FC bare fiber adapters. A preload of 40 KN was applied to the sensor to ensure instantaneous transfer of load to the fiber through the rubber pad assembly. The magnitude of preload was chosen by testing and measuring the stiffness of the testing frame/rubber assembly which was 31985.37 KN/m. The preload is not incorporated in the experimental results since it was not applied in a dynamic manner.

A fixed length of fiber was employed with all sensors. Hence, the effect of sensor length on the dynamic response was not investigated in the present study.

3.5 System Operations

Steps involved in the operation of sensor and system are outlined as follows:

Step 1: He-Ne laser should be turned on at least one hour before the test for laser to reach its stable level.

Step 2: All the system related instruments are turned on: LeCroy 9314 Oscilloscope, *hp* 6235A power supply, photo-detector circuit and amplifier, half hour before the test for the warm up of the system.

Step 3: IBM PC computer with DAS-20 acquisition board are turned on and the data acquisition software is triggered so as to prepare for the collection of data. Also, the sampling rate is selected (those values chosen depend on different loading rate).

Step 4: Specimen is set up in the testing system as shown in Figure 3.1. The loading ram is provided with a metal bar of 20.32 cm (8 inch) in length. This bar is employed for even transmission of the load from the machine to the sensor assembly. Care is taken in centering the sensor with respect to the loading ram for uniform distribution of load intensity along the fiber length.

Step 5: The MTS testing machine is turned on, the error and offset signals are adjusted to zero, and then the necessary parameters in each part of the machine (structure detailed in section 1 of this chapter): are selected by using 458.11 DC controller to set the amplitude (or range) of the applied load, 458.90 generator to simulate the loading condition by controlling the loading rate as well as the loading pattern.

Step 6: Finally, the commencement of the experiment begins by first moving the load cell down manually with 458.20 MicroConsole controller of MTS machine to give the specimen (fiber) a pre-load (40 KN) which can ensure instantaneous transfer of load from the machine to the optical fiber, and

finally the data acquisition is triggered and the loading program is set to start the experiment.

CHAPTER 4

EXPERIMENTAL RESULTS AND ANALYSIS

This chapter gives the experimental results and discussion of load tests for the fiber optic sensor. Two different loading programs, namely a ramp and a step function were chosen for applying time dependent compressive loads to the fiber. Ramp function loads were applied at two different frequencies. Two tests involved applying a relatively slow, quasi-static load for control, and static calibration purposes. Loads were cycled for at least four times for repeatability. Table 4.1, and 4.2 depict the experimental program for the ramp, and step function loading respectively. Loading velocities were controlled by varying the frequency and the value of targeted maximum load amplitudes. For ramp function experiments, two different frequencies of 0.5, and 1 hertz were employed in reaching similar maximum loads. In tables 4.1 and 4.2, loading rate, or velocity is defined as the slope of the applied loading function versus time relationship. Theoretically, for the step function, this slope is infinite. However, from the practical stand point, the slope of the step function possess a finite value, and it can be calculated. This is due to limitations associated with the pumping capacity of the testing machine's hydraulics. The 40 KN pre-load is not incorporated in tables 4.1, and 4.2, since it was not applied in a dynamic manner.

Table 4.1. Experimental program for ramp function, and quasi-static loading

Test No. Designation	Loading Rate (KN/m-sec)	Time to Max Load (sec)	Targeted Max. Load (KN)	Fiber Length (cm)	Targete Max Load per Unit Length (KN/m)	# of Repetitive Cycles
H062309*	2.18	20	8.90	20.32	43.77	4
H062310	43.77	1.00	8.90	20.32	43.77	4
H062311	87.54	0.50	8.90	20.32	43.77	4
H062312	87.54	1.00	17.79	20.32	87.54	4
H062313	175.08	0.50	17.79	20.32	87.54	4
H062314	131.31	1.00	26.69	20.32	131.31	4
H062315	262.62	0.50	26.69	20.32	131.31	4
H062316	175.08	1.00	35.58	20.32	175.08	4
H062317	350.16	0.50	35.58	20.32	175.08	4
H062318	218.85	1.00	44.48	20.32	218.85	4
H062319	437.70	0.50	44.48	20.32	218.85	4
H062322*	2.18	100.00	44.48	20.32	218.85	4

* calibration

Table 4.2. Experimental program for step function loading

Test No. Designation	Loading Rate (KN/m-sec)	Time to Max Load (sec)	Targeted Max Load (KN)	Fiber Length (cm)	Targeted Max Load per Unit Length (KN/m)	# of Repetitive Cycles
H07051	668.08	0.068	2.80	20.32	13.86	4
H07052	988.33	0.068	4.63	20.32	22.76	4
H07053	1625.56	0.076	9.12	20.32	44.94	4
H06232	1562.88	0.076	9.10	20.32	44.79	4
H06233	3112.34	0.076	18.15	20.32	89.29	4
H06234	4434.78	0.076	26.78	20.32	131.75	4
H06235	5864.16	0.076	35.67	20.32	175.52	4
H06236	6718.99	0.076	44.70	20.32	220.02	4

A fixed length of fiber was employed with all sensors. Each test of specimen under different loading condition was assigned a name. Experiments were numbered according to the following scheme, an example in test number H062310, where '**H**' stands for High-Birefringence, '**0623**' corresponds to the date (6/23/94), and '**10**' is designated as the test number.

4.1 Data Analysis

Typical results representing sensor output data in response to the application of ramp function loadings are shown in Figures 4.1 through 4.11. These figures indicate the variation in fringe frequency as a function of loading amplitude and rate. For instance, at lower load intensity amplitudes, as shown in Figs. 4.1 through 4.4, fringe patterns exhibit higher amplitudes and lower frequencies. While the fringe pattern in Fig. 4.5 is preserved as far as the amplitude is concerned, it exhibits a change in frequency. Figures 4.6 through 4.11 are examples of fringe patterns having low amplitudes and high frequencies. The relationship between the fringe and loading is obtained from the experimental data.

For each test, T_f can be computed as the period of the fringe-load relationship (Fig. 2.2). As shown in Figure 4.12, experimental results indicate that the sensor output is dependent both on the loading rate and amplitude. At first glance, data pairs in Fig. 4.12 insinuate that similar load amplitudes induce nearly the same number of fringes irrespective of the loading velocity. However, loading

rate insensitivity diminish for increasing loading velocities (Figure 4.13). In fact, T_f varies with loading amplitude as well as its velocity. A single calibration factor such as T_f alone is not sufficient for accurate prediction of dynamic loads. This can be illustrated by attempting to predict the magnitude of dynamic loads with a T_f which is calculated based on a single quasi-static test (Table 4.3).

We performed two tests for the purpose of calibration (test No. H062309, and H062322 in Table 4.3). Both of the experiments were performed at the same quasi-static rate of 2.18 KN/m-sec. These experiments yielded two different calibration factors of 10.80 and 11.97 KN/m per fringe for test no. H062322, and H062309 respectively. As these results indicate, relative errors in the computation of predicted dynamic loads are highly dependent on the calibration load amplitude (Table 4.3). Hence, T_f is influenced both by the magnitude, and velocity of the loading, and it can not be employed as calibration factor.

4.2 Experimental Calibration and Results

Our experimental results indicate that the linear regression of fringe data for the range of dynamic loads provides a more rational calibration approach. Results of regression analysis for the range of ramp function loads are depicted in Figure 4.14. In Figure 4.14, k stands for the number of observed fringes at maximum load. As results indicate in Table 4.3, computation based on the regression relationship provided the least error in the prediction of dynamic loads.

4.3 Discussion

Application of very high loading rates were accomplished by a series of step forcing functions (Table 4.2). Figures 15 through 22 illustrate typical results obtained from such experiments. It is not possible to directly determine the load from fringe data as the fringe pattern is aperiodic. One way to remedy this is to further employ the regression relationship developed earlier (Fig. 4.14) for the computation of loads from the fringe data. To examine the applicability of such an approach, data in Fig. 4.13 was linearly extrapolated to a T_f value of zero. The loading rates at or beyond a T_f value of zero may be interpreted as loading velocities that are too fast for the development of fringe patterns. For our sensor configuration, we arrived at a critical loading velocity of 1652 KN/m-sec (Fig. 4.13). Step function response data was subsequently analyzed based on the linear regression approach, and results are presented in Table 4.4. As evident by these results, error in the computation of the dynamic loads are less severe at lower velocities (lower than 1600 KN/m-sec). However, the generated error is too large for arriving at any conclusions pertaining to the computation approach. Our experimental parameters were limited by the hydraulic components of the testing system, and therefore, we could not achieve intermediate loading rates at the amplitudes employed in this thesis.

Table 4.3 Comparison of predicted load intensities

Test No Designation	No. of Fringes to Max. Load	Max. Applied Load Intensity (KN/m)	Computed Load Intensity (KN/m), based on T_f = 10.80 KN/m per fringe	Computed Load Intensity (KN/m), based on T_f = 11.97 KN/m per fringe	Computed Load Intensity, based on Regression (KN/m)
H062309[1]	3.90	47.23	42.10	46.7	47.0
H062310	3.55	43.60	38.40	42.50	43.2
H062311	3.43	42.32	37.0	41.0	42.00
H062312	7.34	85.38	79.20	87.80	83.25
H062314	11.35	127.70	122.60	135.80	125.46
H062313	7.08	82.82	76.50	84.70	80.43
H062316	15.50	169.90	167.30	185.40	169.25
H062318	19.90	212.54	214.90	238.0	215.6
H062315	10.97	123.85	118.50	131.20	121.50
H062317	15.00	165.09	162.0	179.50	164.0
H062319	19.28	206.45	208.20	230.70	209.1
H062322[2]	19.99	217.40	216.0	239.30	216.7

1 calibration test, T_f = 11.97 KN/m per fringe

2 calibration test, T_f = 10.80 KN/m per fringe

Table 4.4 Comparison of the applied and computed loads for step function loading of the optical fiber

Test No	Loading Rate (KN/m-sec)	Total No.of Fringes to Max. Load	Max. Applied Load per Unit Length (KN/m)	Max. ComputedLoad per Unit Length (KN/m)	Relative Error (%)
H07051	668.0	0.53	13.0	11.40	12.80
H07052	988.30	1.18	22.90	18.20	20.40
H07053	1625.60	1.51	45.0	21.70	51.50
H06232	1562.90	3.25	45.0	40.0	11.30
H06233	3112.30	3.50	89.30	42.60	52.30
H06234	4434.80	2.50	131.75	32.10	75.60
H06235	5864.20	3.50	175.50	42.60	75.70
H06236	6719.0	4.50	220.0	53.11	75.80

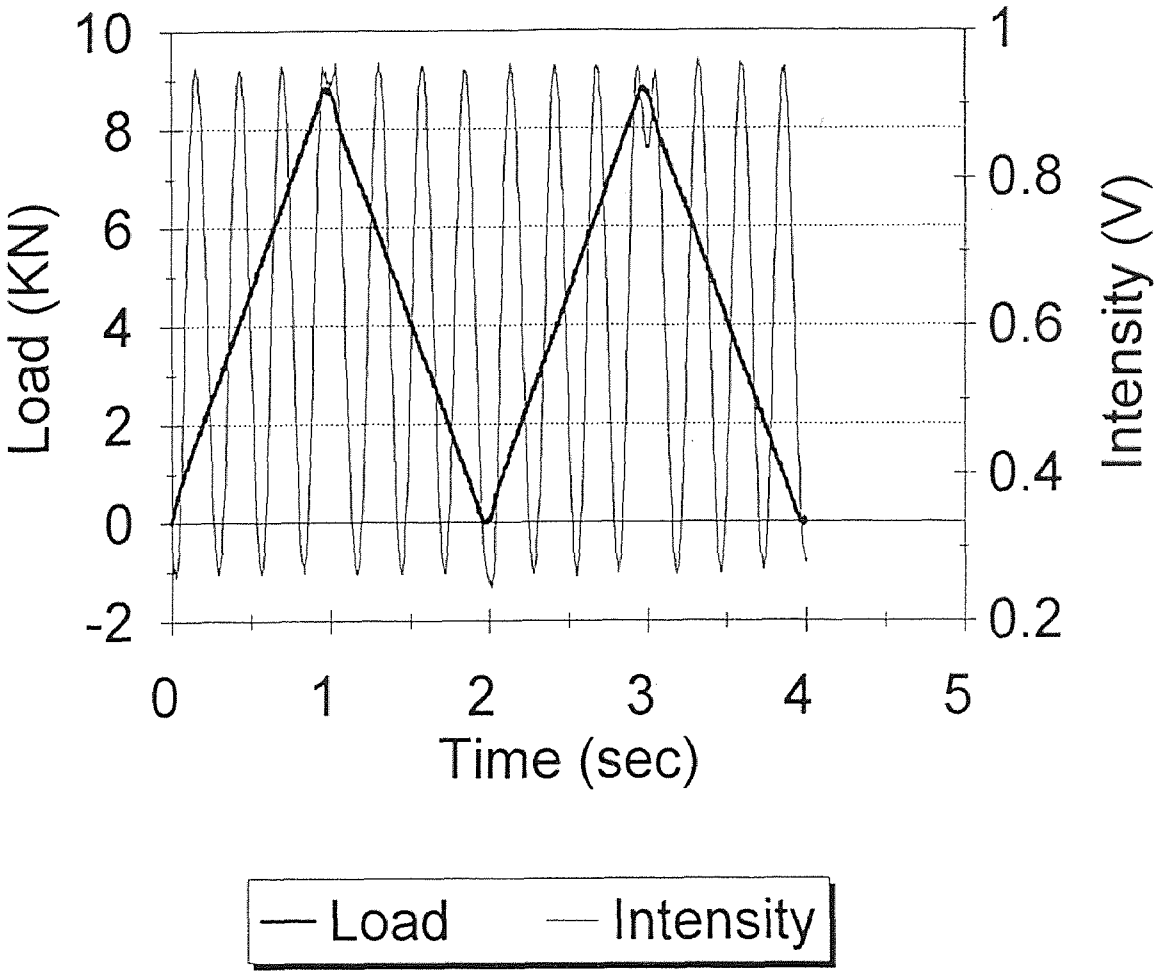

Figure 4.1 Applied ramp function with fiber intensity output for test H062310

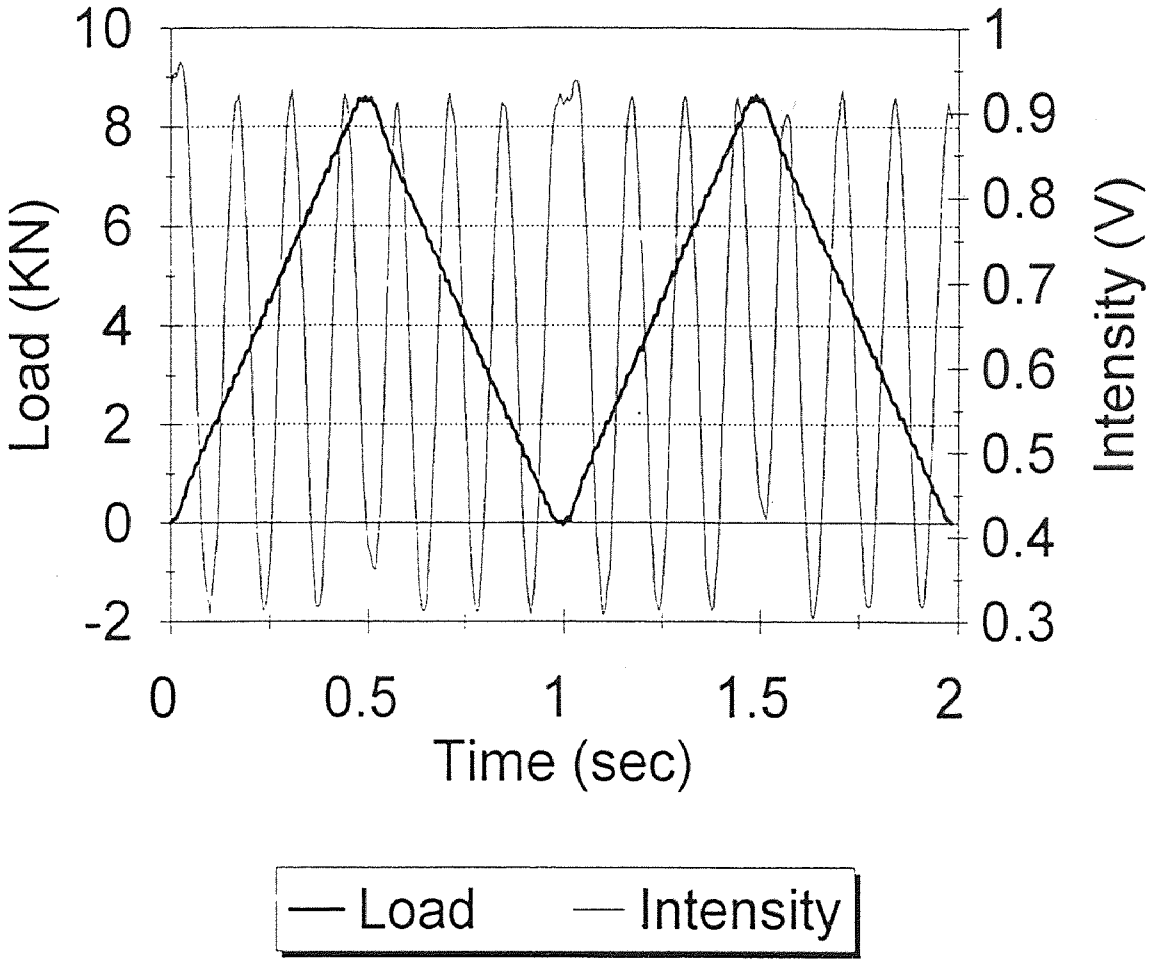

Figure 4.2 Applied ramp function with fiber intensity output for test H062311

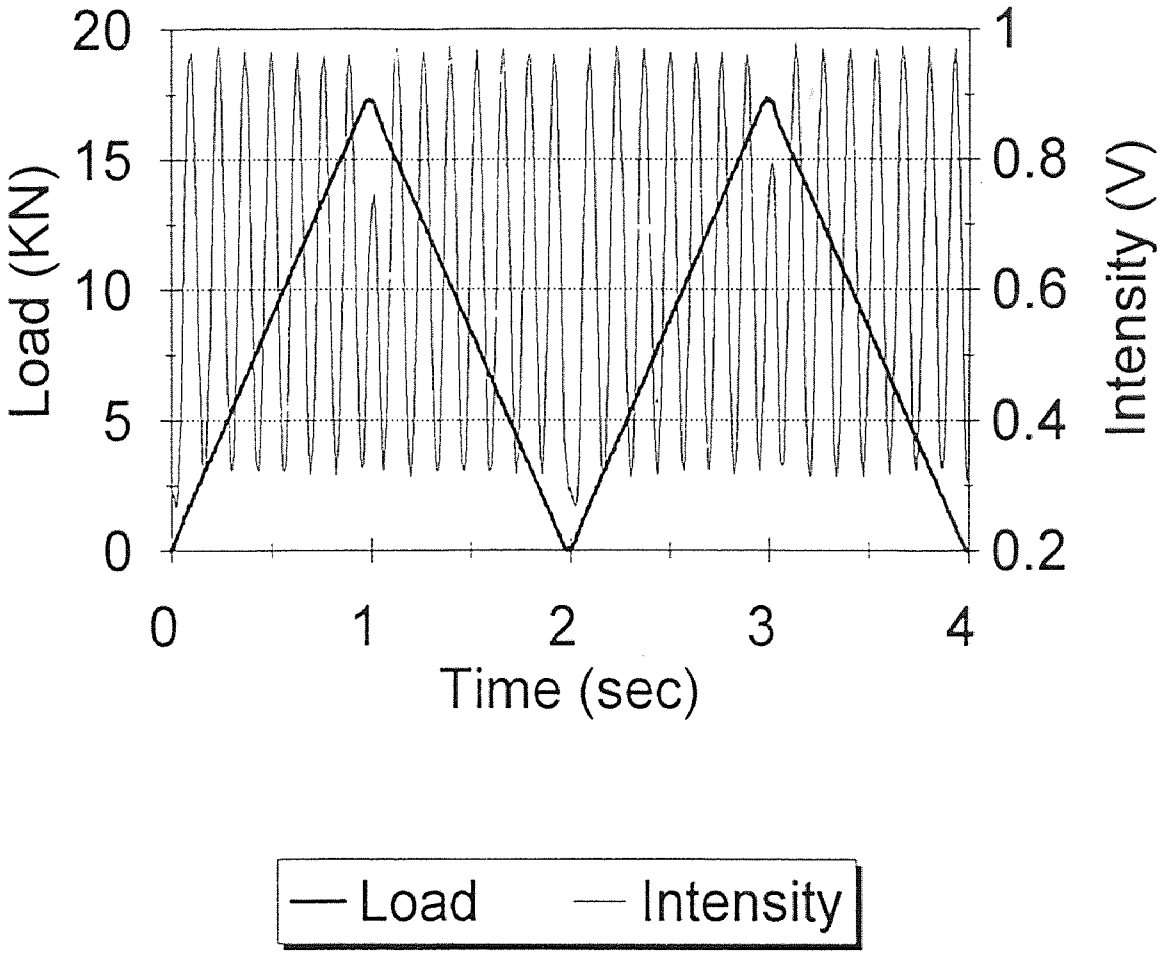

Figure 4.3 Applied ramp function with fiber intensity output for test H062312

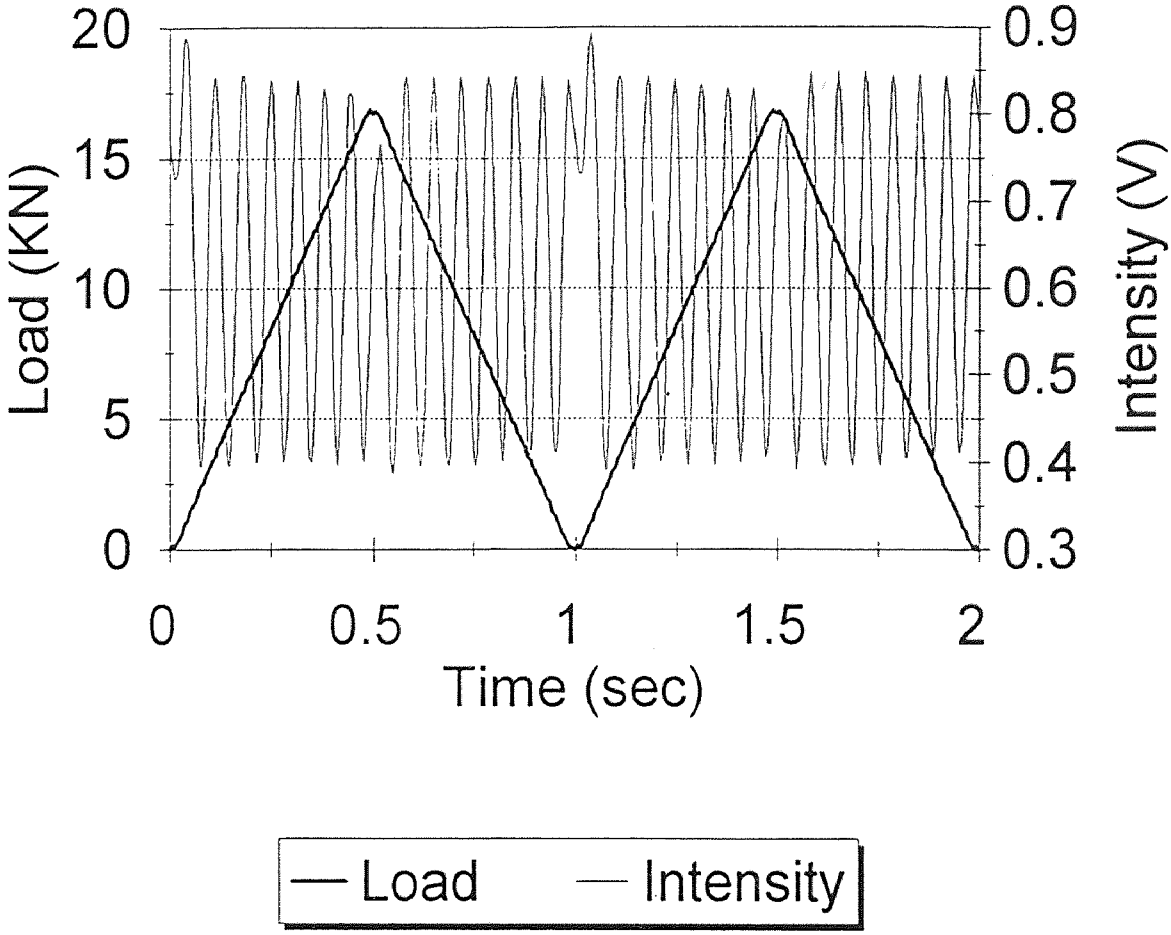

Figure 4.4 Applied ramp function with fiber intensity output for test H062313

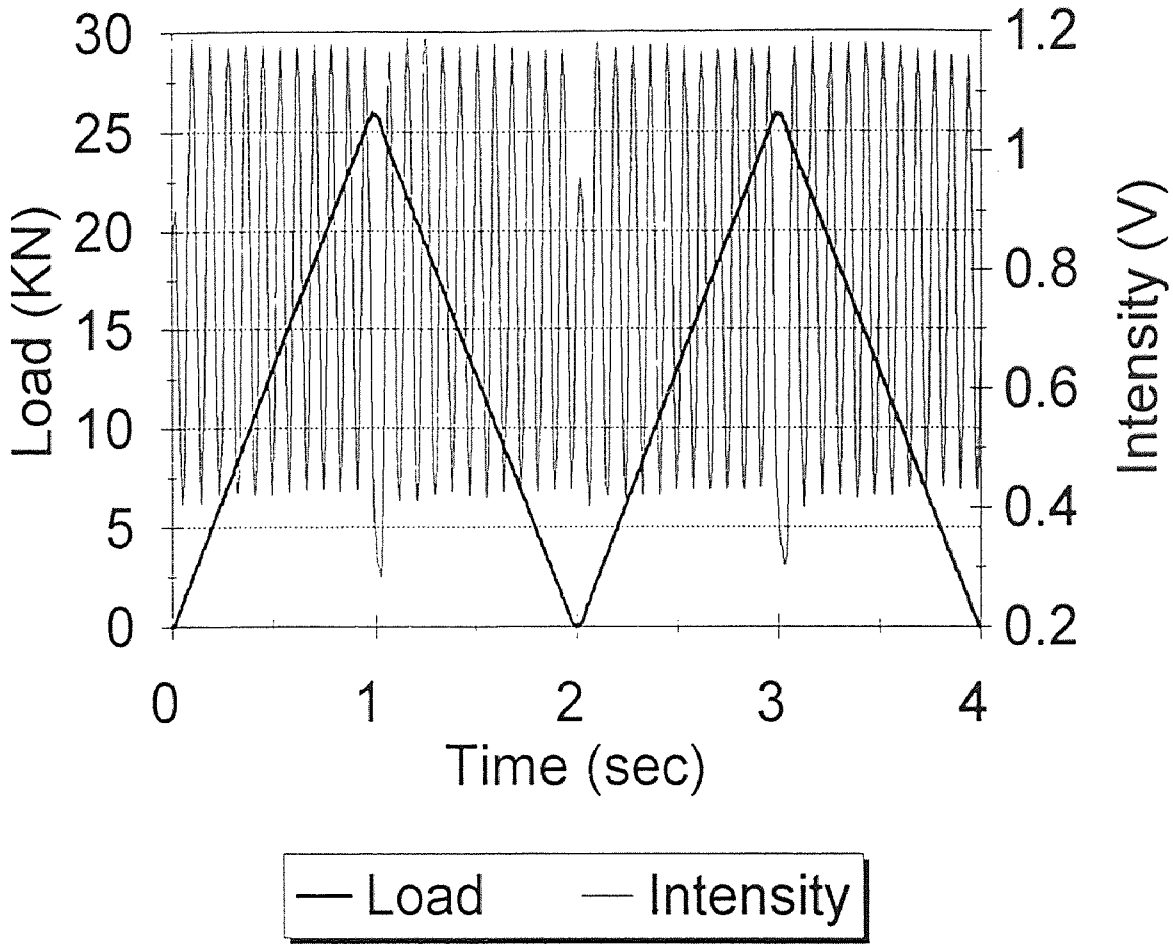

Figure 4.5 Applied ramp function with fiber intensity output for test H062314

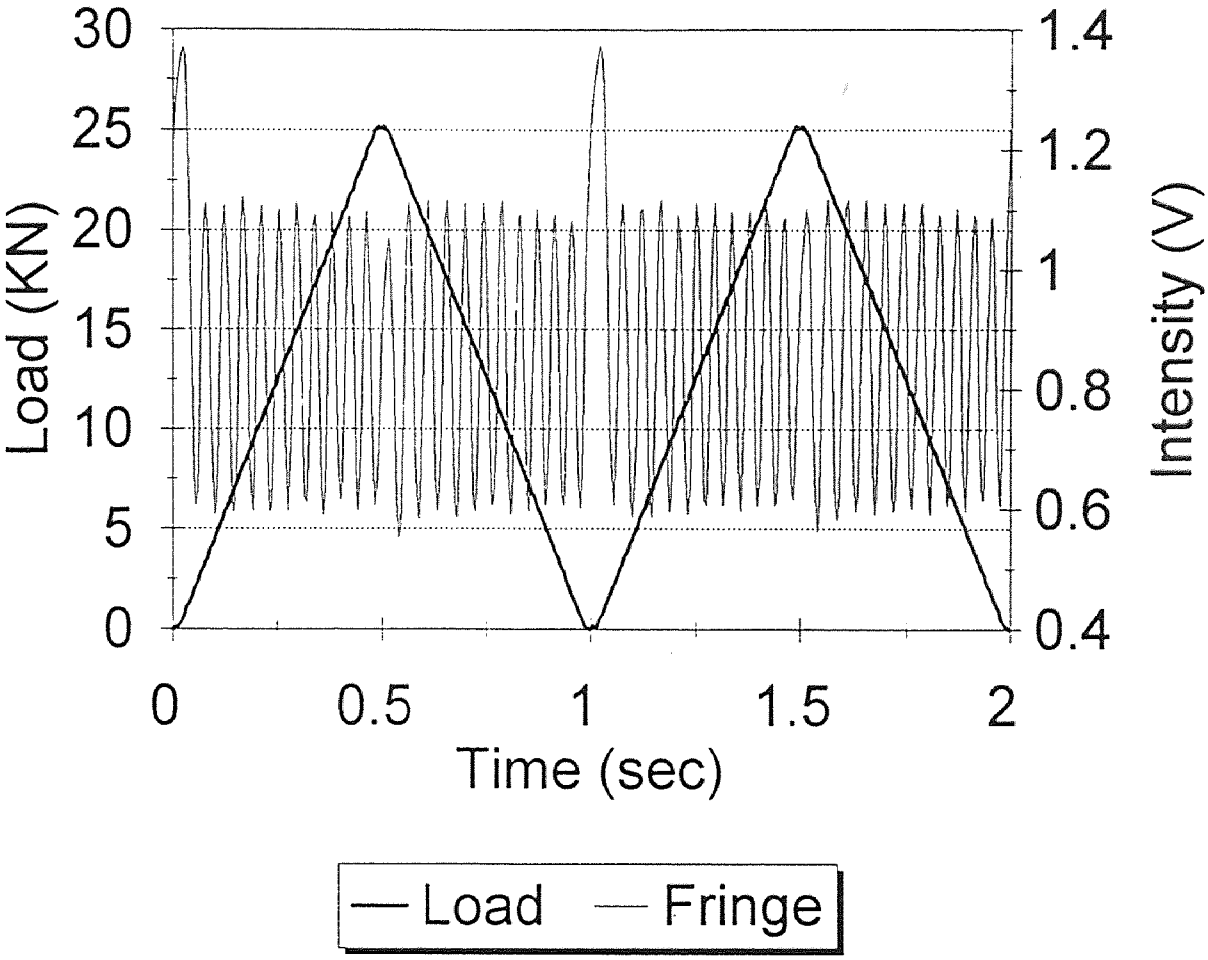

Figure 4.6 Applied ramp function with fiber intensity output for test H062315

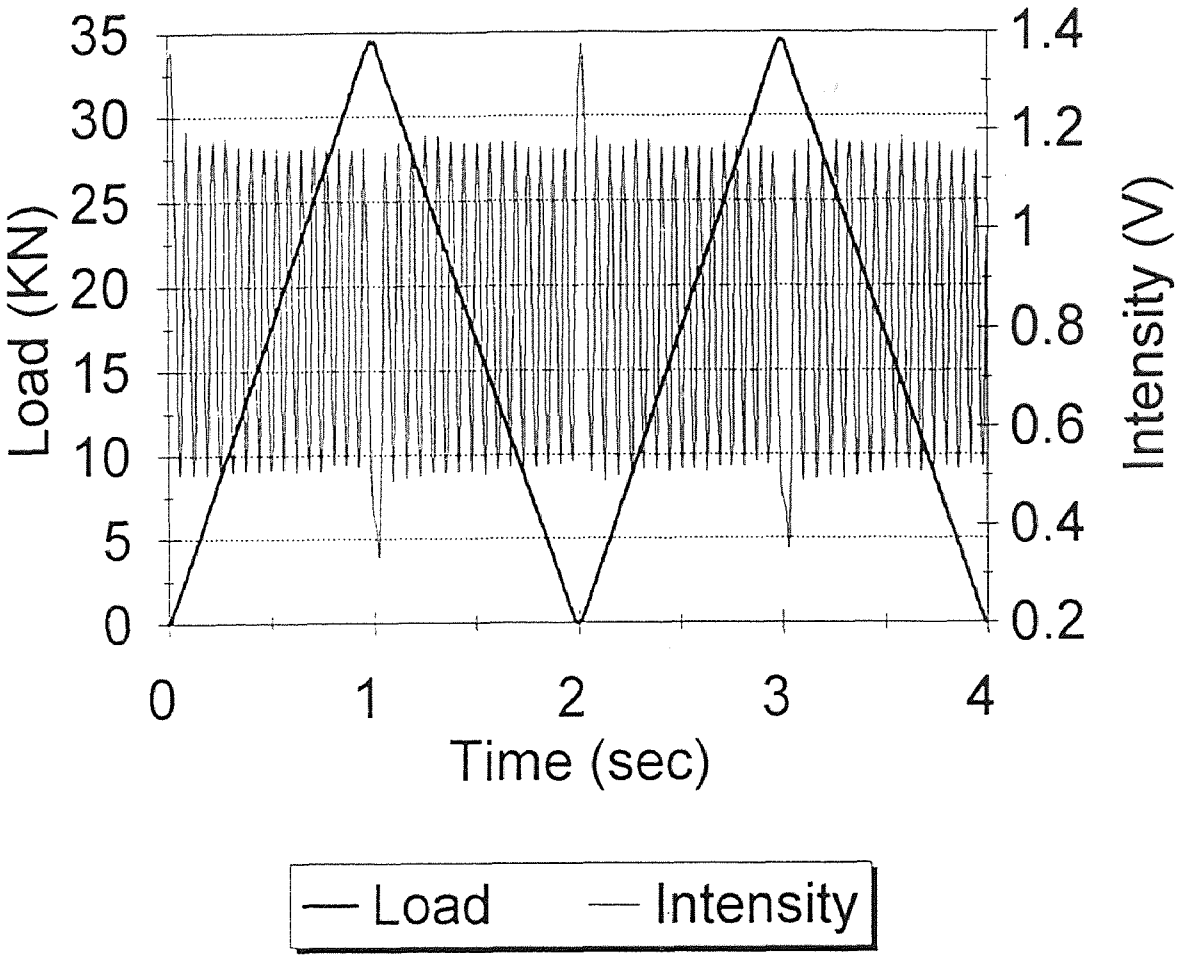

Figure 4.7 Applied ramp function with fiber intensity output for test H062316

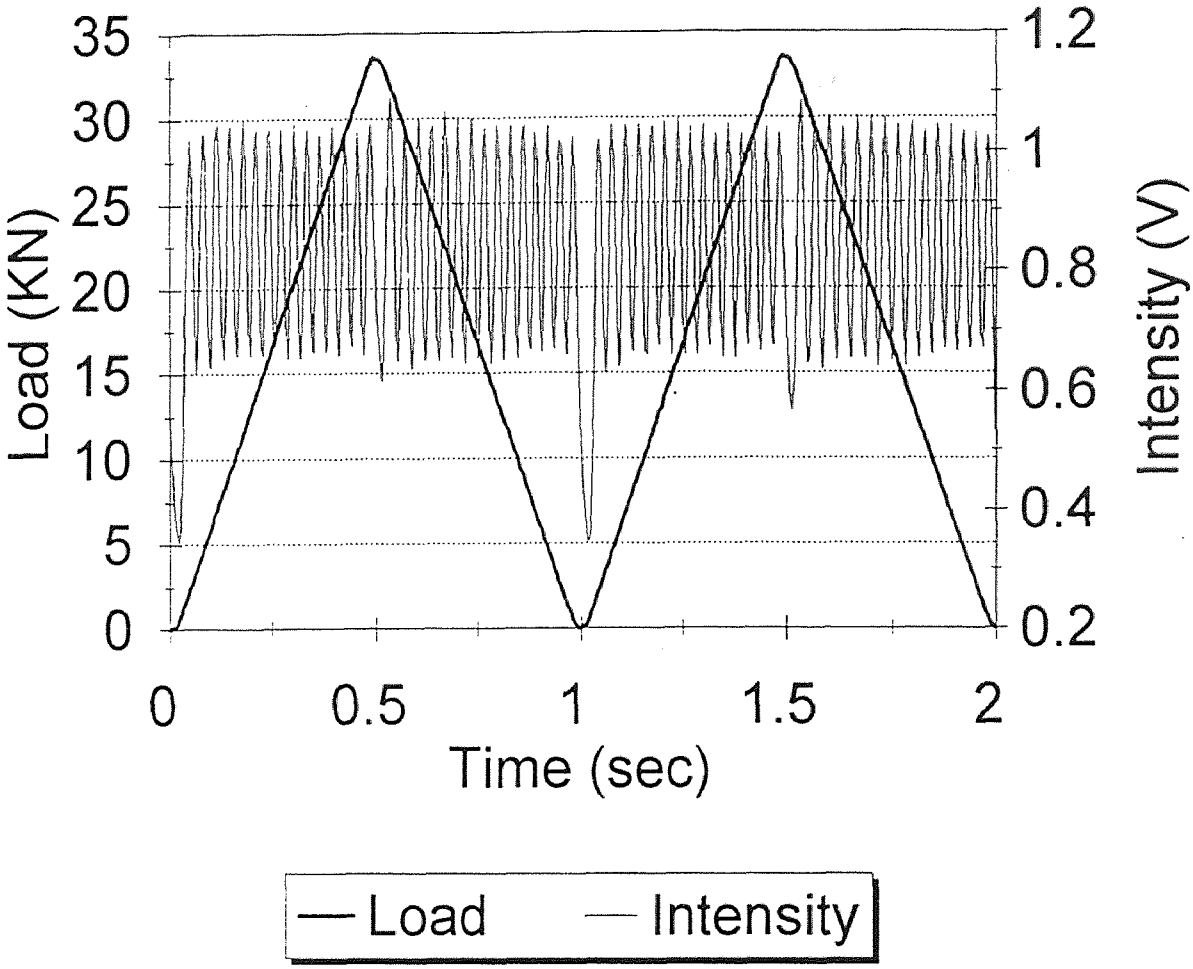

Figure 4.8 Applied ramp function with fiber intensity output for test H062317

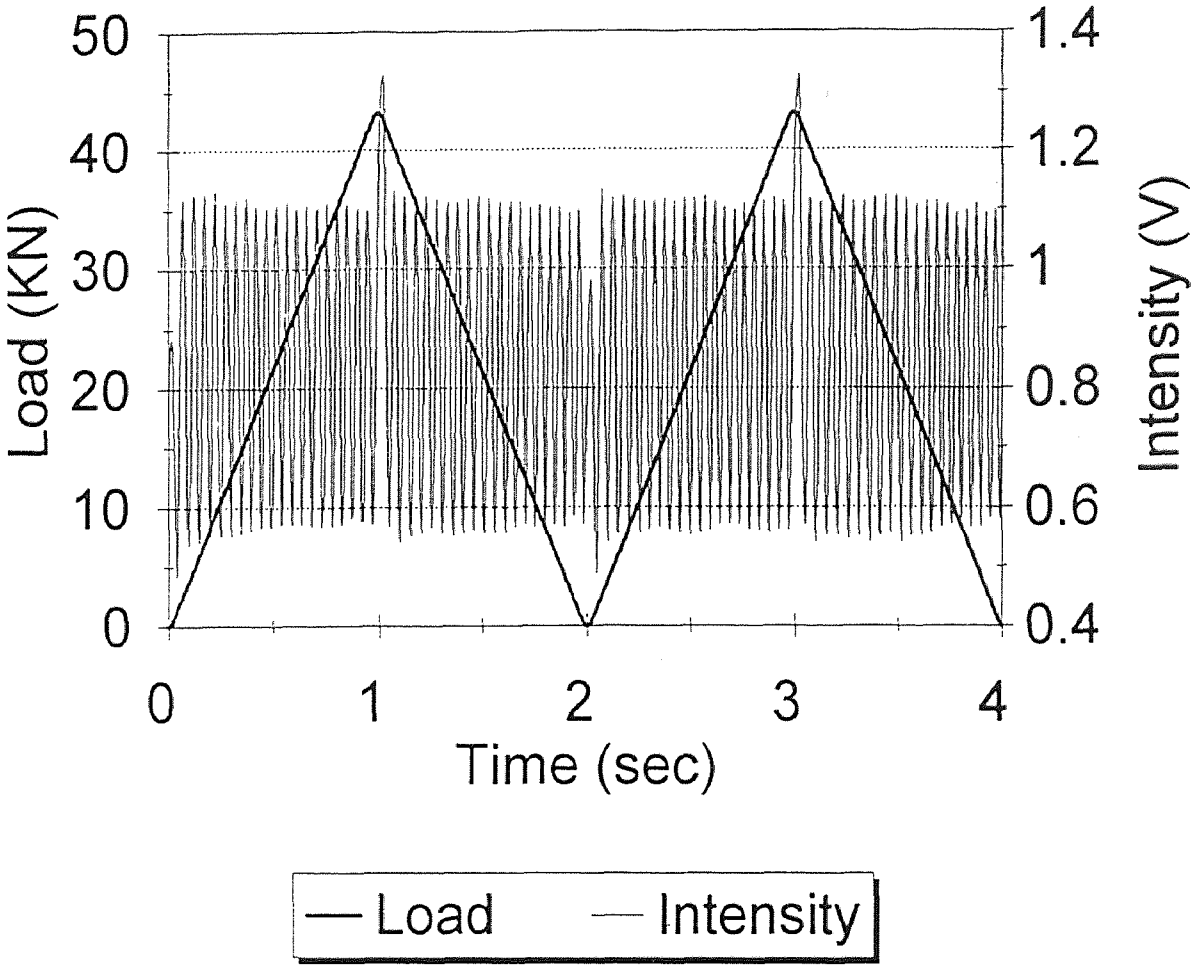

Figure 4.9 Applied ramp function with fiber intensity output for test H062318

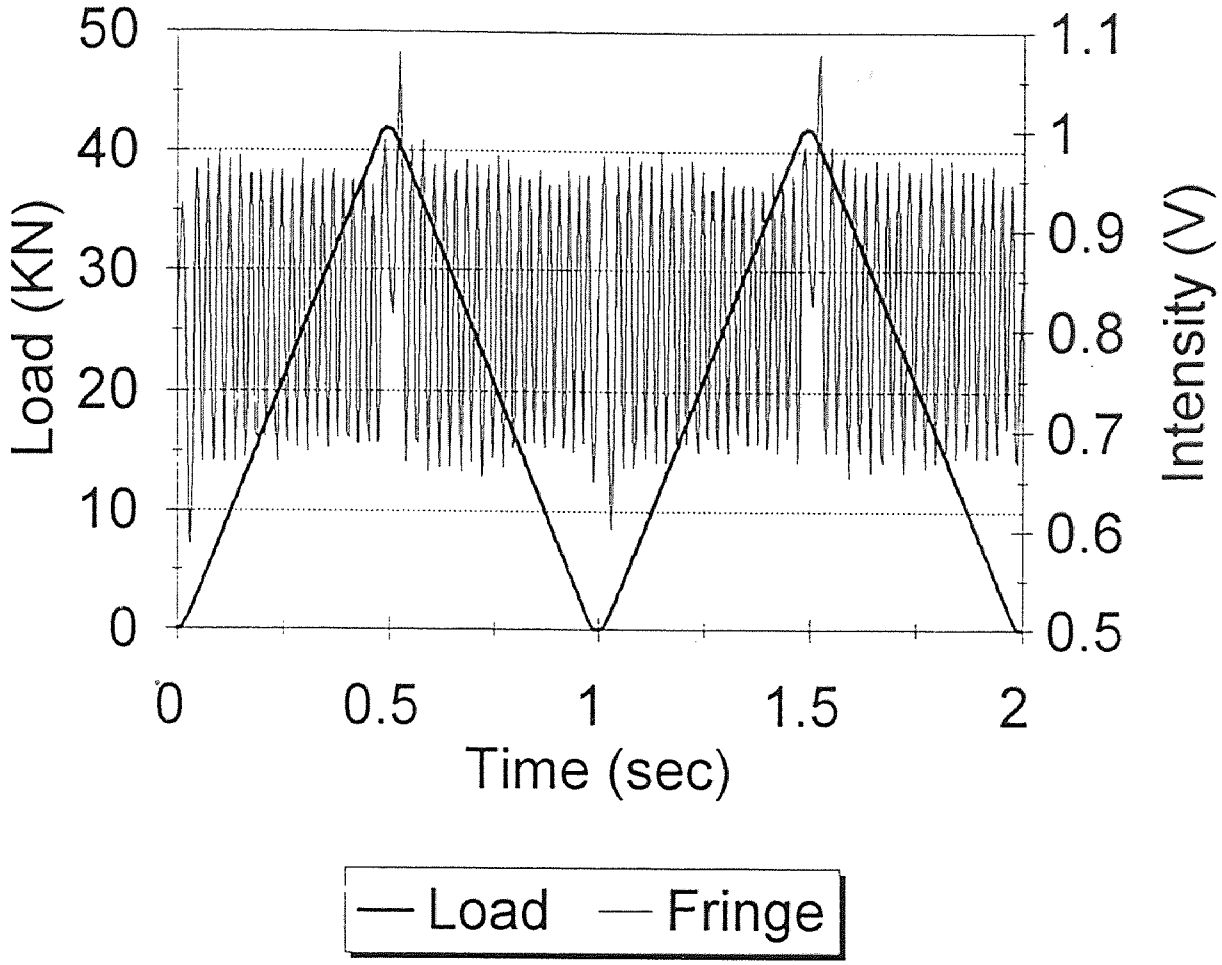

Figure 4.10 Applied ramp function with fiber intensity output for test H062319

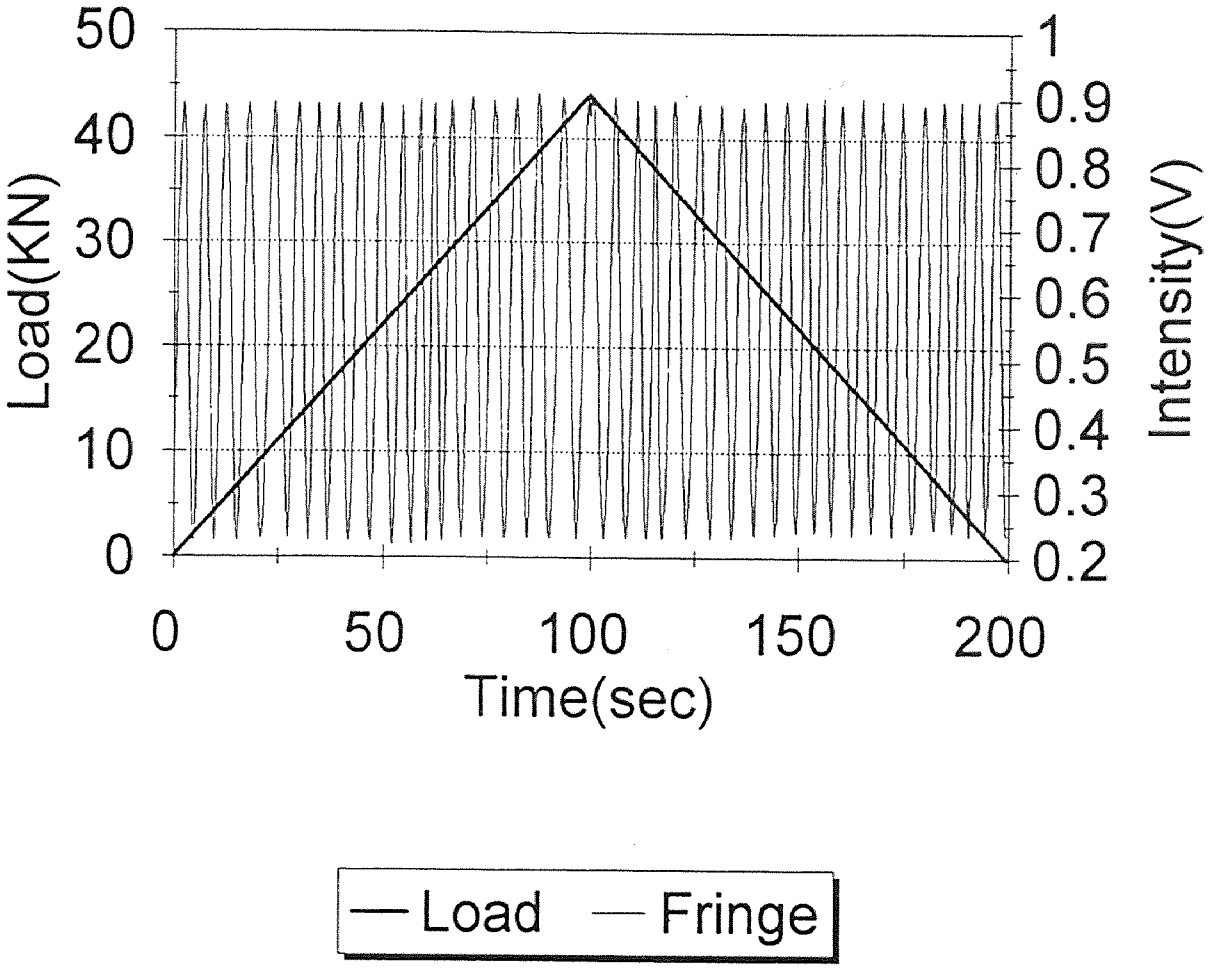

Figure 4.11 Applied ramp function with fiber intensity output for test H062322

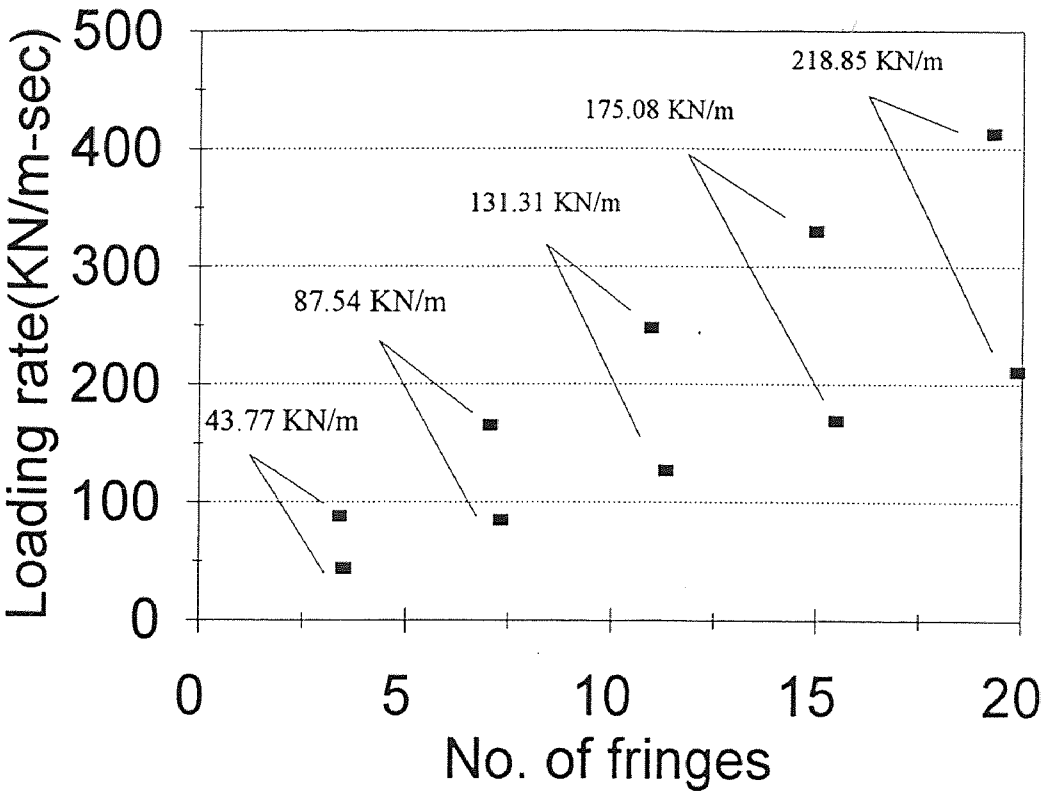

Figure 4.12 Rate of loading versus number of observed fringes

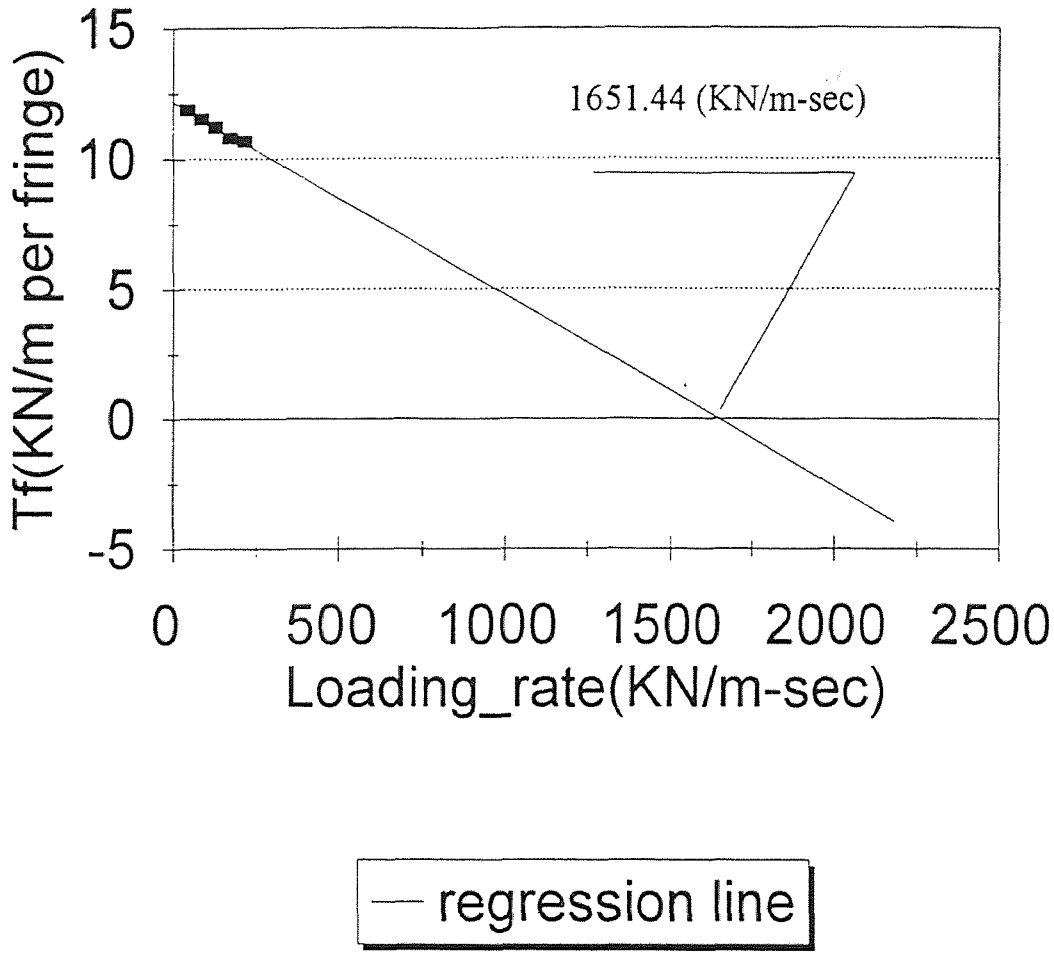

Figure 4.13 Variation of the calibration factor with loading rate

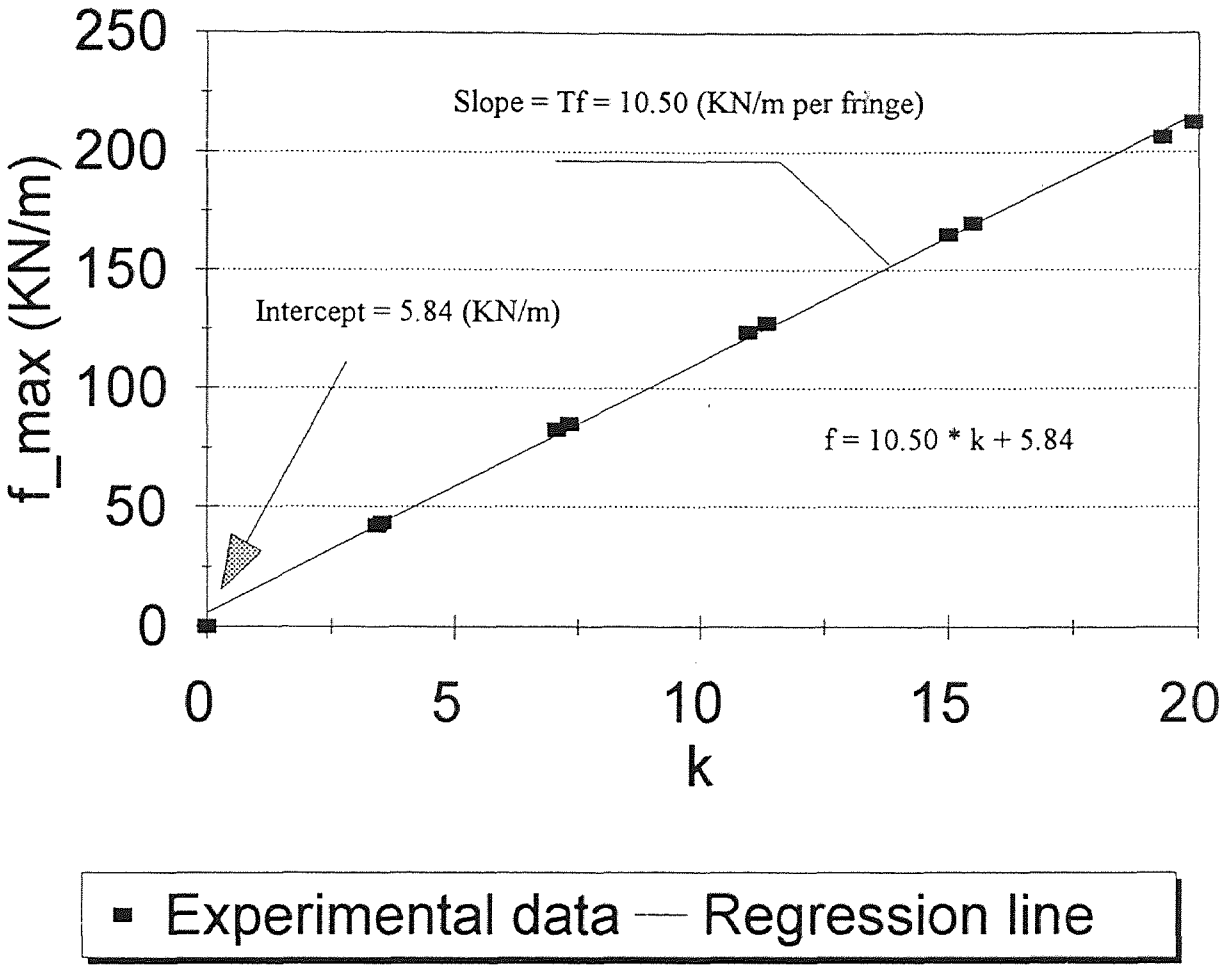

Figure 4.14 Regression analysis of load intensity versus fringe data

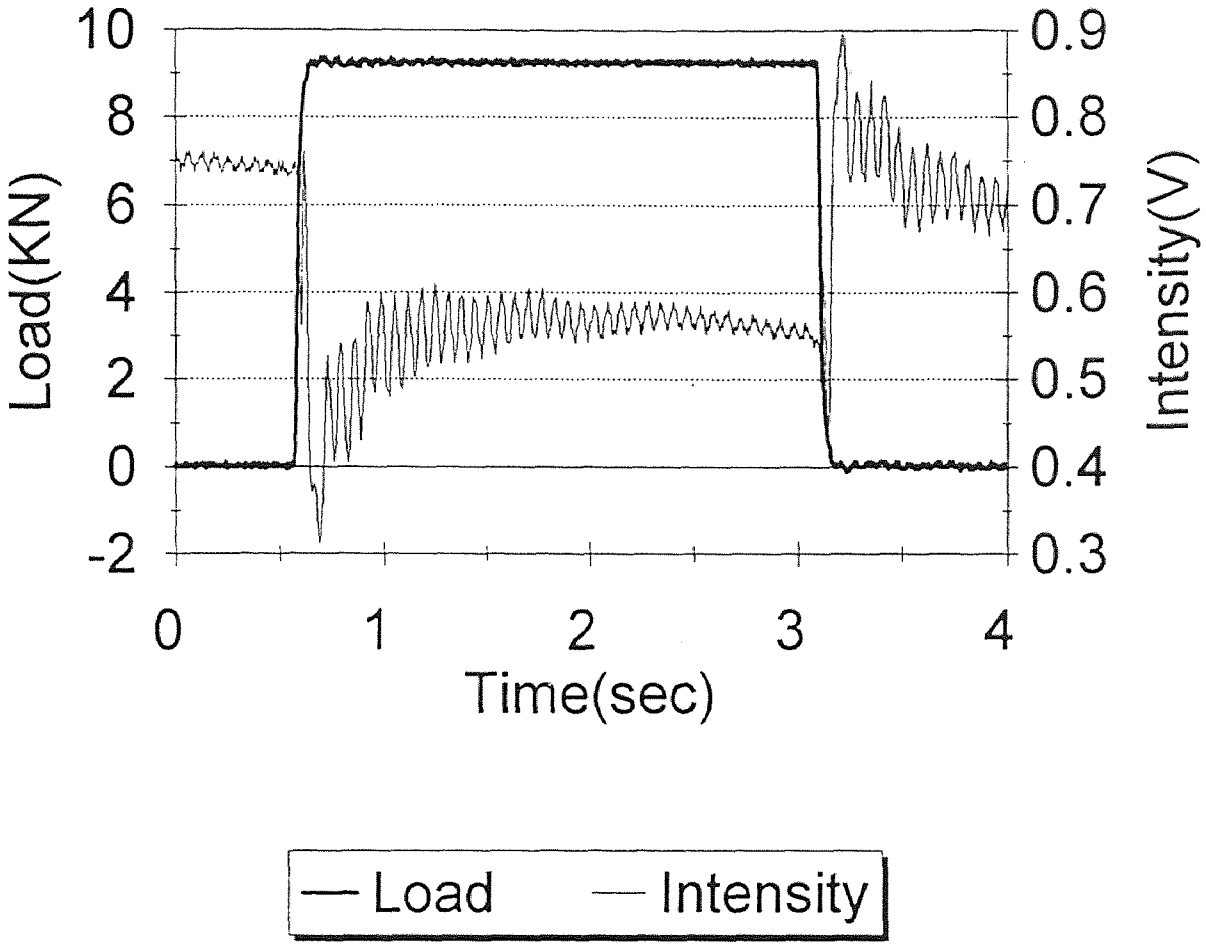

Figure 4.15 Applied step function with fiber intensity output for test H06232

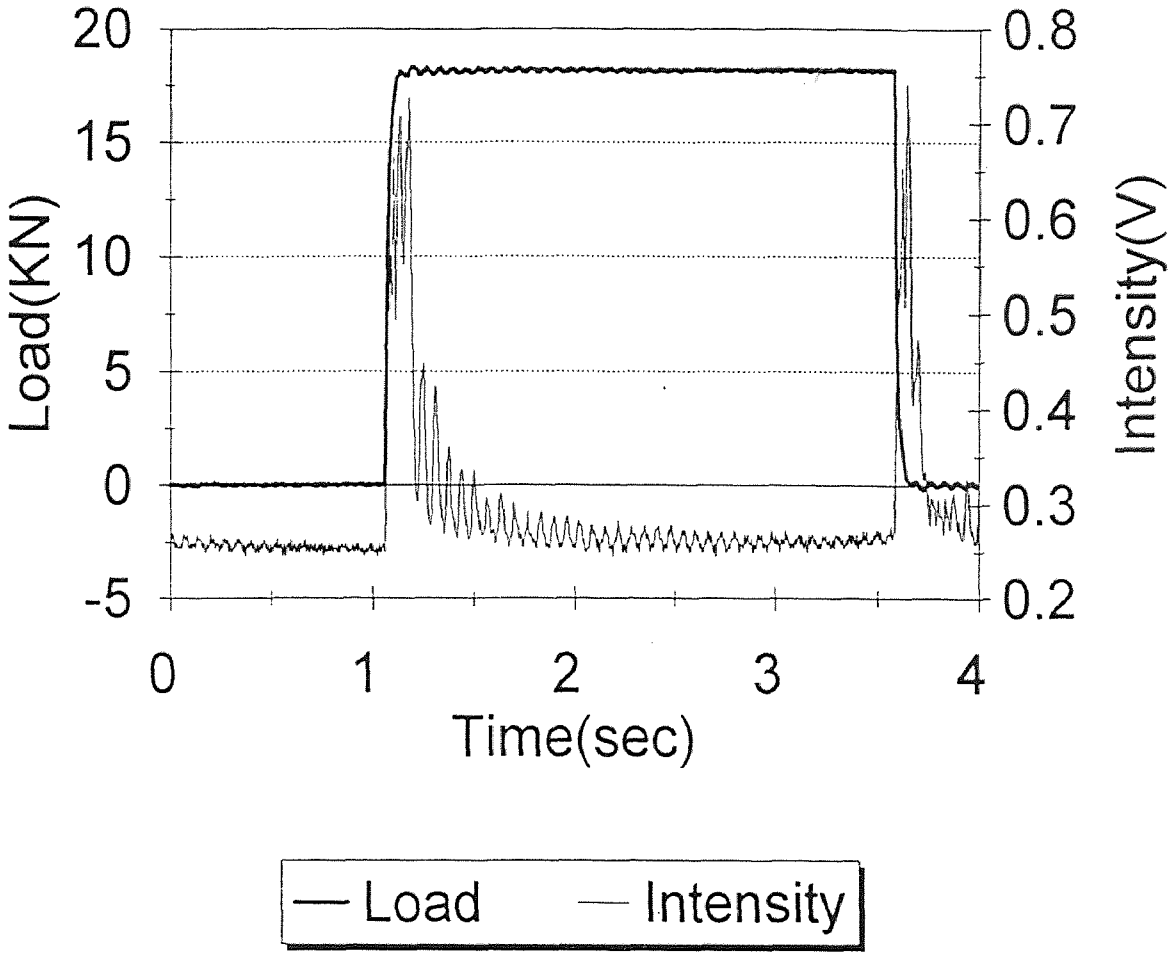

Figure 4.16 Applied step function with fiber intensity output for test H06233

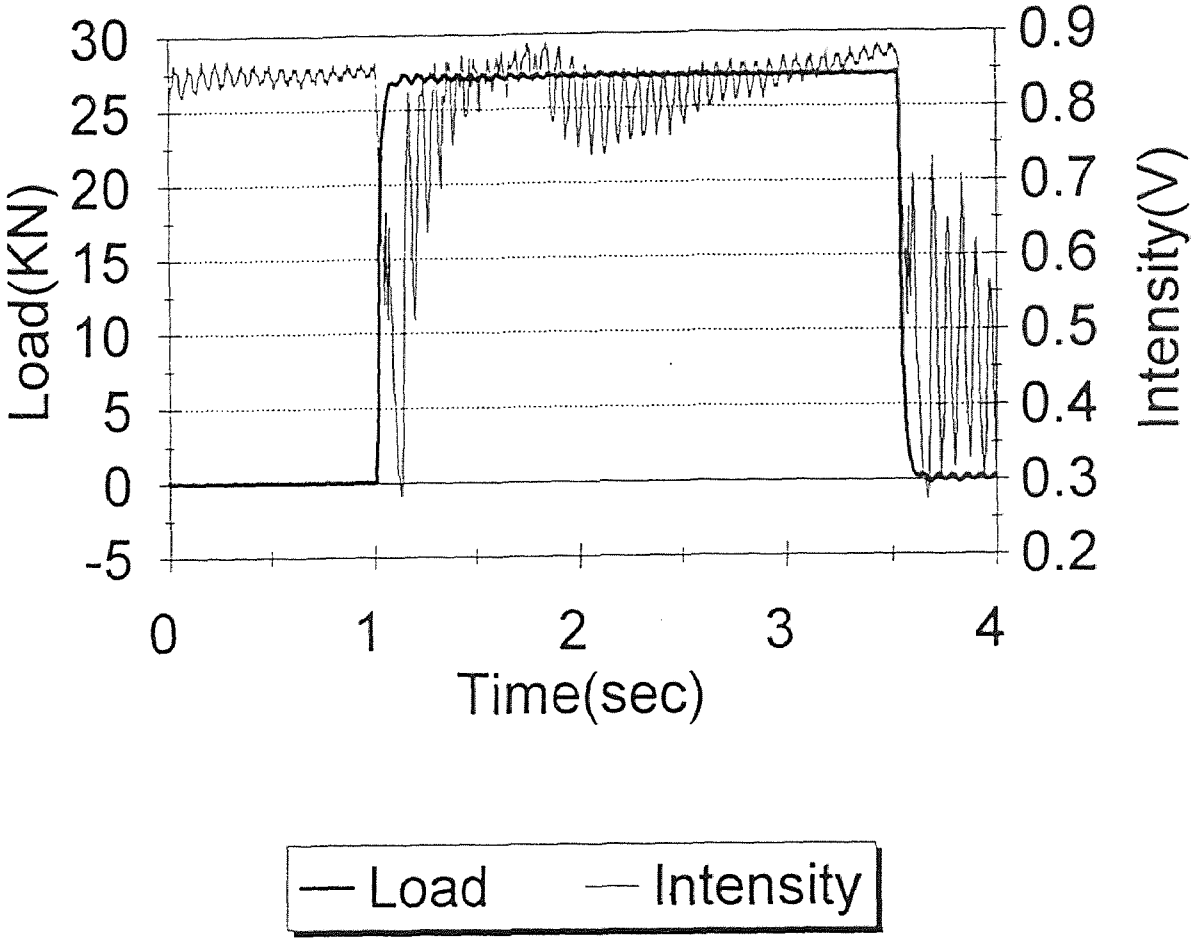

Figure 4.17 Applied step function with fiber intensity output for test H06234

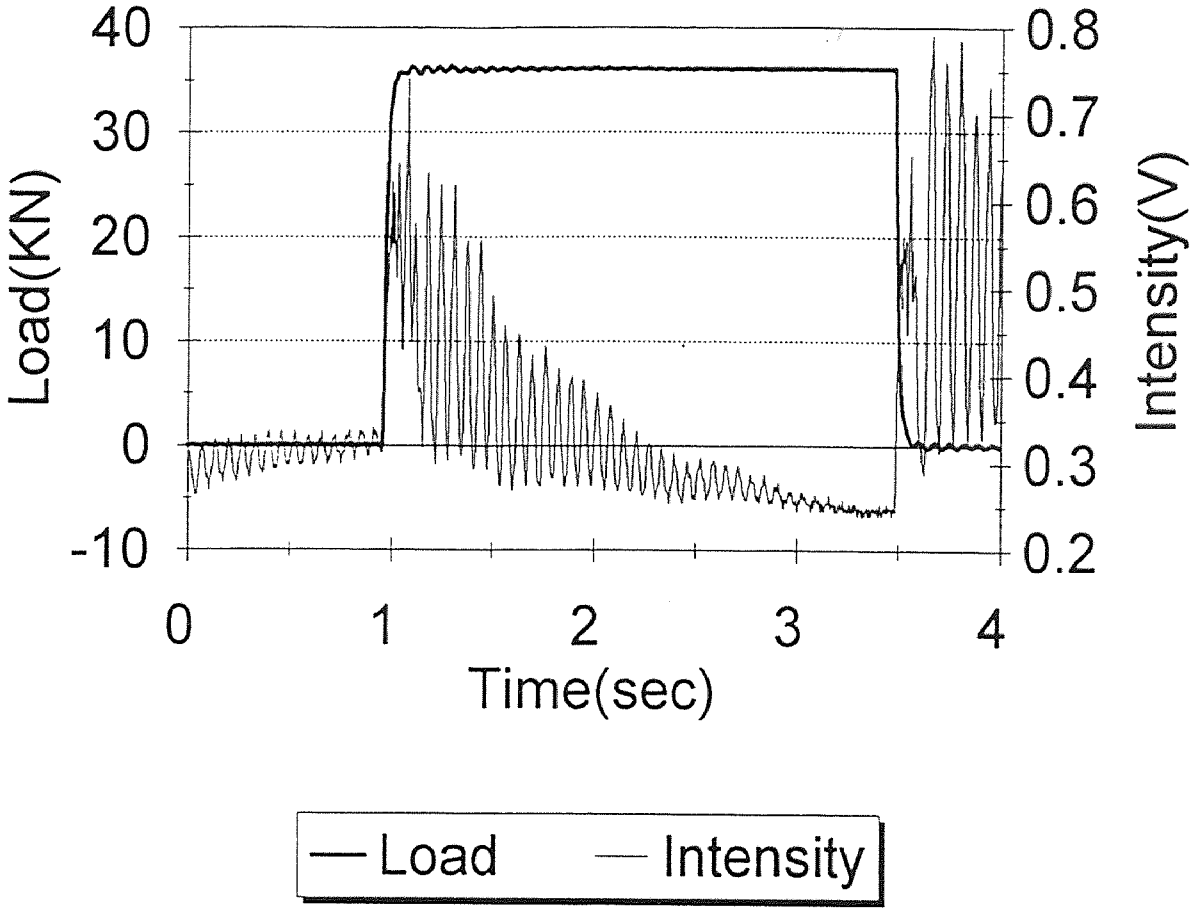

Figure 4.18 Applied step function with fiber intensity output for test H06235

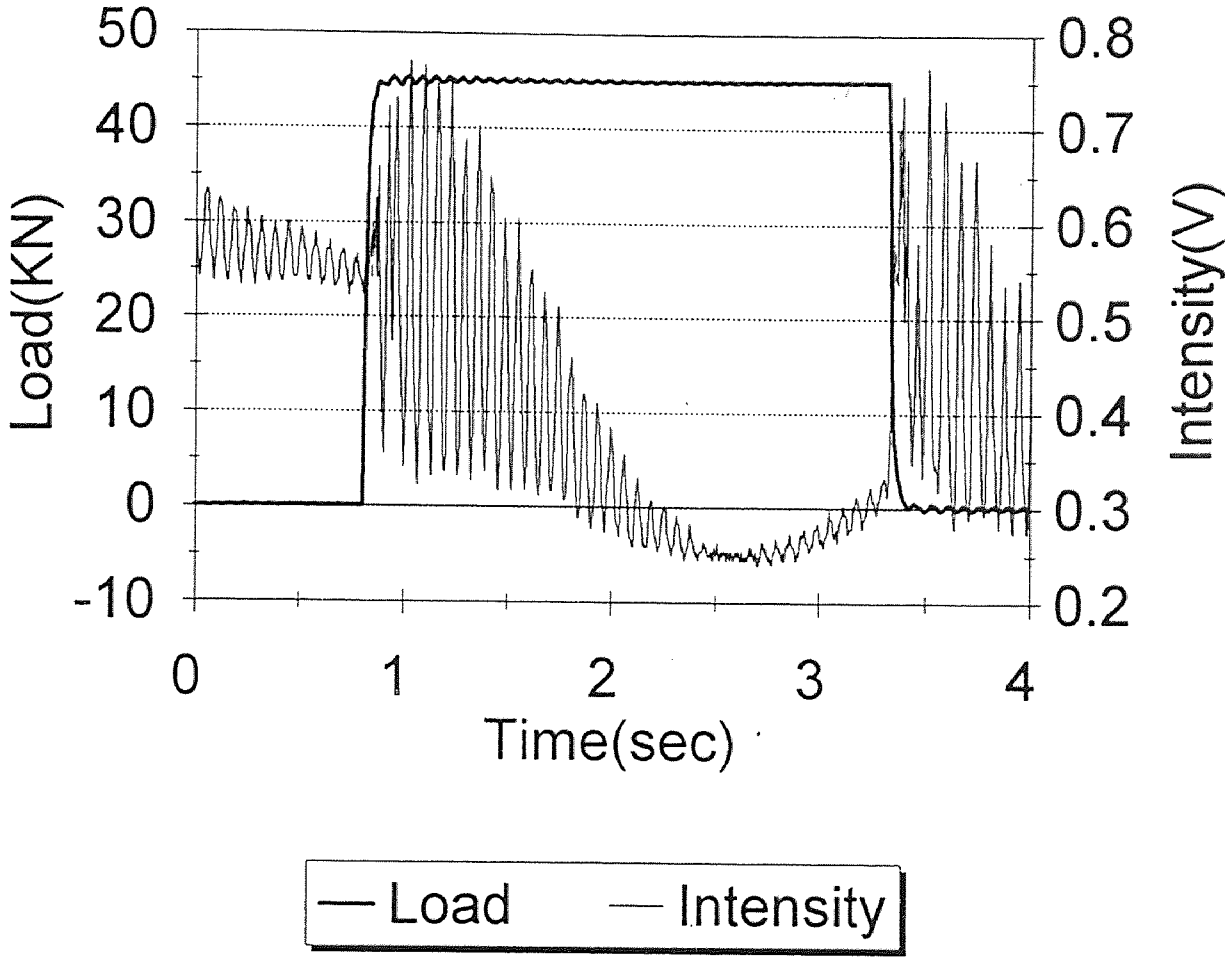

Figure 4.19 Applied ramp function with fiber intensity output for test H06236

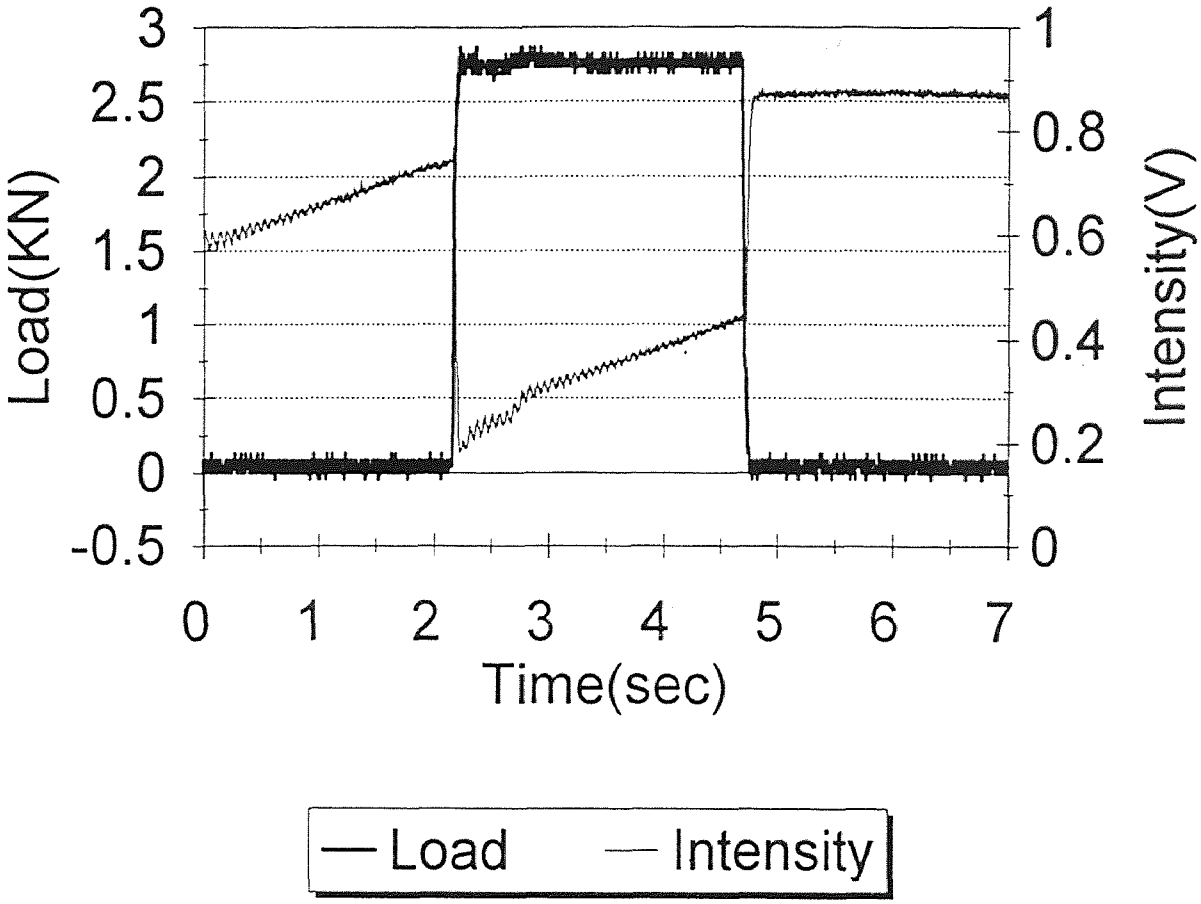

Figure 4.20 Applied ramp function with fiber intensity output for test H07051

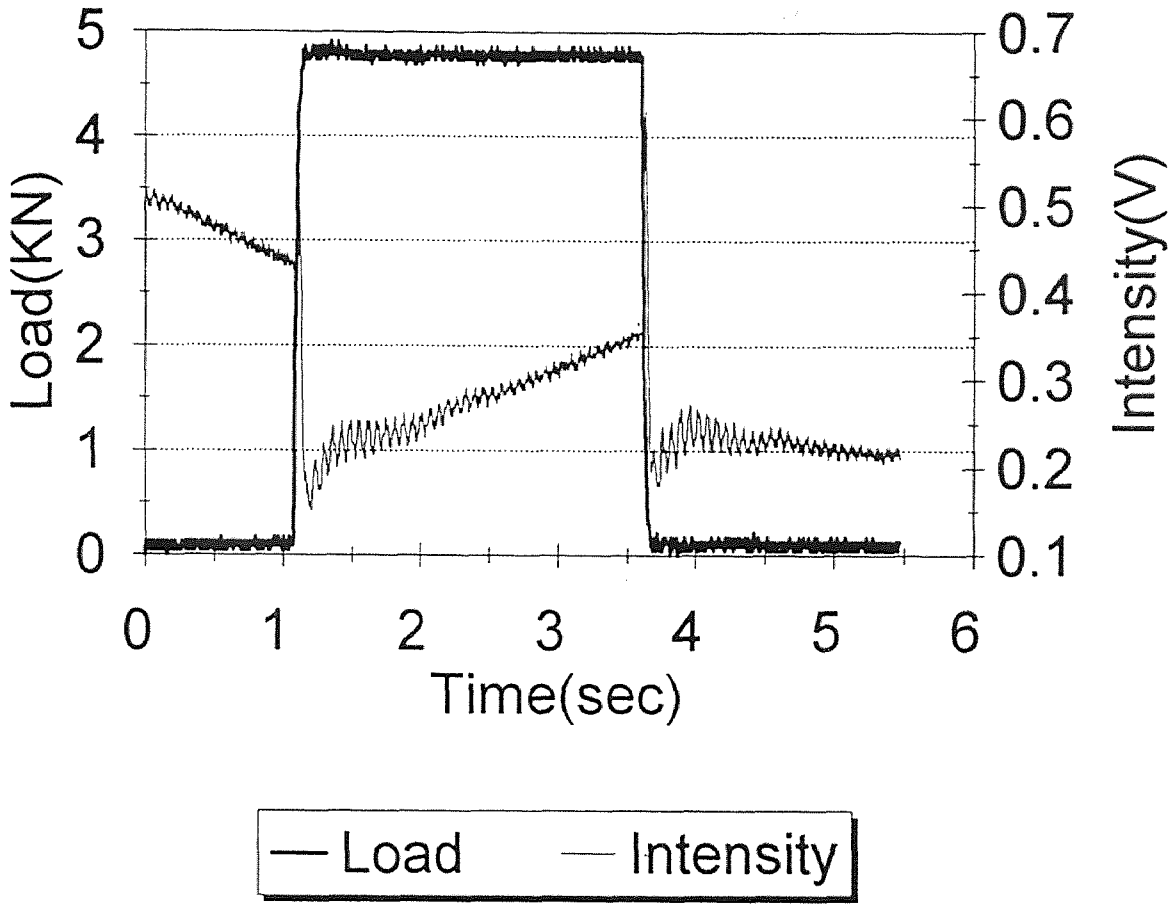

Figure 4.21 Applied ramp function with fiber intensity output for test H07052

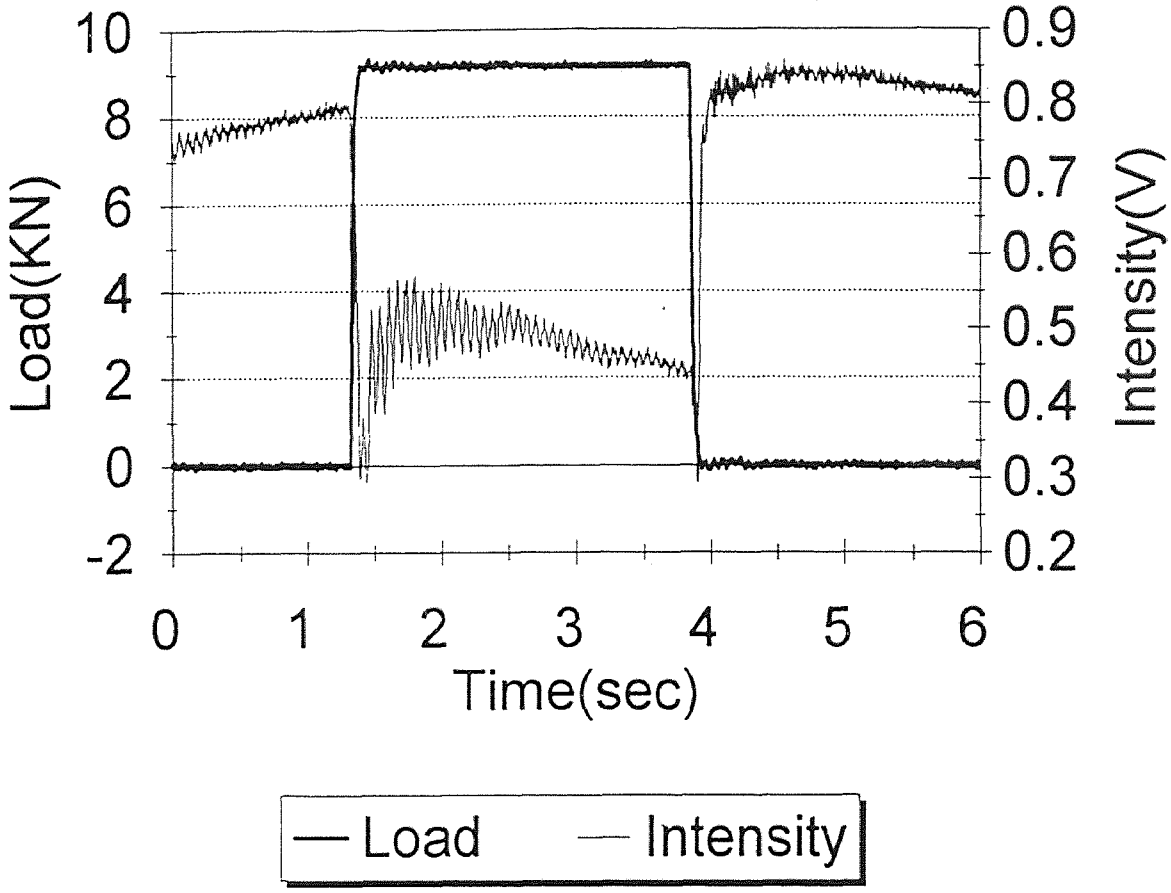

Figure 4.22 Applied ramp function with fiber intensity output for test H07053

CHAPTER 5

CONCLUSIONS

Results presented in this study clearly indicate that it is possible to accurately measure the magnitude of dynamic compressive loads with the proposed sensor. Output of the sensor is a function of the amplitude as well as the velocity of applied loading. Therefore, within the spectrum of desired velocities, calibration of the sensor should be achieved through regression analysis. The ramification of this finding is that T_f by itself does not represent the calibration factor for these sensors. This further implies that Eqs. (2.24) and (2.25) shall be modified through replacement of T_f with regression parameters. Hence, the following relationship is suggested for relating the change in beat length to f:

$$\frac{1}{L_B} = \frac{1}{L_{B_0}} + \frac{f - c}{L_0 T_f} \tag{5.1}$$

where, T_f is the slope of the regression line, and c is the intercept and has the units of force per unit length. The relationship between k and T_f is given as:

$$T_f = \frac{f - c}{k} \tag{5.2}$$

By substituting the results of regression analysis in Eqn. (5.1), it is possible to monitor the change in beat length for the optical fiber as a function of load intensity. For instance, substitution of the regression analysis parameters from present study's data into Eqn. (5.1), yields the following relationship for which the results are given in Figure 5.1:

$$\frac{1}{L_B} = \frac{1}{L_{B_0}} + \frac{f - 0.40}{L_0 T_f} \tag{5.3}$$

In Eqn. (5.3), L_{B_0} is equal to 1.16 mm, and the zone between L_{B_0} of 1.16 mm and the first data point in Fig. 5.1 corresponds to the previously mentioned static pre-load of 40 KN (Chap. 3). In using Eqn. (5.2), one should note that it is of general form, and the regression parameters c, and T_f pertain to the particular sensor characteristics (fiber length, type etc.), and loading conditions.

A fixed length of fiber was employed with all sensors, hence, the effect of sensor length on the sensor response was not investigated in the present study. Therefore, this issue shall be further investigated in future research. Another issue which deserves further attention is the development of a testing program to carry on experiments covering a wider spectrum of loading rates.

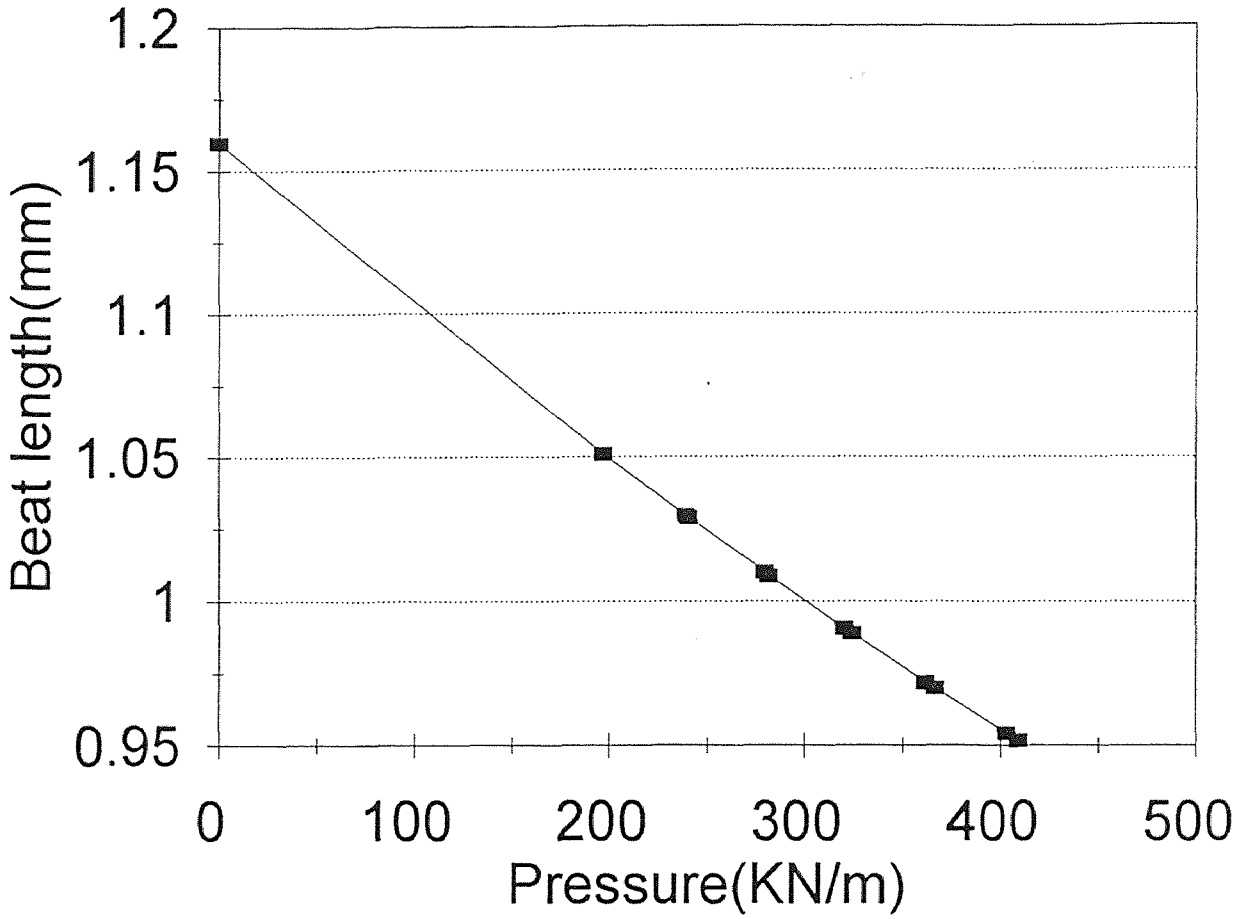

Figure 5.1 Relation between beat length of fiber and applied load intensity

APPENDIX

Programming List for Calculating the Number of Fringes

```
/*** wjp, fringe.c is to develop a software which can automatically
                calculate the number of fringes from intensity(nfringe),
                the loading speed (frequence),
                to calibration( kips_per_second),
                input--- from h*.* like h05305g1.prn or h0530141.prn
                output---on the screen with 'dtime', 'nfringe',
                        'calibration', 'frequence', 'max_load' ****/

#include <stdio.h>
#include <stdlib.h>
#include <graph.h>
#include <string.h>
#include <io.h>
#include <math.h>

#include "dlf.h"

#define MIN -1
#define MAX 1

int main()
{ FILE *file_ptr, *fp, *time_ptr;
 char *file_in;
 float time, load, intensity;
 float tmp_t, tmp_l, tmp_i, tmp;
 float min_load, max_load, min_time, max_time, dtime, begin_time, end_time;
 float min_intensity, max_intensity, end_intensity;
 float nfringe, first_fringe, last_fringe, frequence, calibration;
 int s, light, sl;
 int i, j;   /* how many times the fringe changes */

 int t;
 int menu();

 _clearscreen( _GCLEARSCREEN );

 while( (t=menu())==1 )
 {   _clearscreen( _GCLEARSCREEN );

 printf( "\n\nPlease enter your data file: ");
 gets( file_in );

 printf("\n\n\nThe input file is \'%s\'", file_in );
```

```
/** file which stores original data **/
if( (file_ptr=fopen(file_in, "rt")) == NULL )
 { _clearscreen( _GCLEARSCREEN );
  printf( "\n\nData file could not be opened.\n" );
  exit( 0 );
 };



/** file which will be used to store the result **/
if( (fp=fopen("c:\\wjp\\hb\\0622.prn", "a+")) == NULL )
 { _clearscreen( _GCLEARSCREEN );
  printf( "\n\nData file could not be opened.\n" );
  exit( 0 );
 }

i=0; j=0;

fscanf( file_ptr, "%f%f%f", &time, &load, &intensity ); /* get first data */
tmp_t = time;   min_time = time;  begin_time = time;
tmp_l = load;   min_load = load;
tmp_i = intensity; min_intensity = intensity;
fringe[i].sp = intensity; period[j].sp = time;
light = MIN;

s = 0;   /** 0 for begin, 1 for up, -1 for down **/
while( !feof(file_ptr) )
 { fscanf( file_ptr, "%f%f%f", &time, &load, &intensity );
  tmp = intensity - tmp_i;          /* to decide when one fringe reachs the end */
  if( s==0 )
       {
        if( tmp > 0 )
          { s = 1;
          }
        else
          { s = -1;
          }
       }

  if( (s==1 && tmp>=0) || (s==-1 && tmp<=0) )  /* case between two end */
       { end_time = time;           /* in case of reaching the end of file */
        max_load = load;
        end_intensity = intensity;
        tmp_t = time;
        tmp_l = load;
        tmp_i = intensity;
       }
  else if( s==1 && tmp<0 )        /* case which reaches the top */
          { s = -1;
           end_time = time;        /* in case of reaching the end of file */
           max_load = load;
           if( light == MIN )
                { fringe[++i].sp = tmp_i;
                  max_intensity = tmp_i;
```

```
                period[++j].sp = tmp_t;
                max_time = tmp_t;
                light = MAX;
               }
          else
               { fringe[++i].sp = tmp_i;
                min_intensity = tmp_i;
                period[++j].sp = tmp_t;
                min_time = tmp_t;
                light = MIN;
               }
          end_intensity = intensity;
          tmp_i = intensity;
          tmp_t = time;
          tmp_l = load;
          fringe[--i].distance = fabs(max_intensity - min_intensity);
          ++i;   /* distance and startpoint has one step gap */
          period[--j].distance = fabs(max_time - min_time);
        /**      fprintf( time_ptr, "%12f%12f\n", period[j].sp, period[j].distance ); **/
          ++j;
         }
         else if( s==-1 && tmp>0 )          /* case which reaches bottom */
               { s = 1;
                end_time = time;  /* in case of reaching the end of file */
                max_load = load;
                if( light == MIN )
                 { fringe[++i].sp = tmp_i;
                      max_intensity = tmp_i;
                      period[++j].sp = tmp_t;
                      max_time = tmp_t;
                      light = MAX;
                 }
                else
                 { fringe[++i].sp = tmp_i;
                      min_intensity = tmp_i;
                      period[++j].sp = tmp_t;
                      min_time = tmp_t;
                      light = MIN;
                 }
                end_intensity = intensity;
                tmp_i = intensity;
                tmp_t = time;
                tmp_l = load;
                fringe[--i].distance = fabs(max_intensity - min_intensity);
                ++i;
                period[--j].distance = fabs(max_time - min_time);
          /**   fprintf( time_ptr, "%12f%12f\n", period[j].sp, period[j].distance ); **/
                ++j;
               }
 }
/* end of recursive */


if( light == MIN )                  /* to store the last point */
```

```
 { fringe[i++].distance = fabs(end_intensity - min_intensity);
  period[j].distance = fabs(end_time - min_time);
 /*      fprintf( time_ptr, "%12f%12f\n", period[j].sp, period[j].distance ); */
 }
else
 { fringe[i++].distance = fabs(end_intensity - max_intensity);
  period[j].distance = fabs(end_time - max_time);
 /* fprintf( time_ptr, "%12f%12f\n", period[j].sp, period[j].distance ); */
 }
/*** j=number of fringe - 1 ***/


/*** to calculate the fringe number ***/
first_fringe = (fringe[0].distance>=fringe[1].distance)?1:(fringe[0].distance/fringe[1].distance);
last_fringe = (fringe[i-1].distance>=fringe[i-2].distance)?1:(fringe[i-1].distance/fringe[i-2].distance);
nfringe = first_fringe + i - 2 + last_fringe;


/*** to calculate the other reference ***/

calibration = fabs(max_load - min_load)/nfringe;
dtime = end_time - begin_time;
frequence = fabs(max_load - min_load)/dtime;



printf( "\n\nNumber of fringes = %f", nfringe );
printf( "\n\nCalibration = %f (kips/fringe)", calibration );
printf( "\n\nfrequence = %f (kips/sec)", frequence );







/***************************************
if( sl == 1 )
 { printf("\n\nMaximum load = %f (kips)", max_load );
 }
else
 { printf("\n\nMaximum load = %f (kips)", min_load );
 }                          ****************************************/

max_load = fabs( max_load - min_load );
printf("\n\nMaximum load = %f (kips)", max_load );


fprintf( fp, "\n%12f%12f%12f%12f%12f", dtime, nfringe, calibration, frequence, max_load );

printf("\n\nThis is the end of test.");


}
```

```
 fcloseall();
 exit( 0 );
}

/*****************************************************************/



int menu()
{   char ch;

    printf("\n\nDo you want to enter another file(y/n): ");
    ch=getch();

    return( (ch=='y')?1:0 );

}
```

REFERENCES

1. R.C. Jones, *J.Opt. Soc. Am.*,31, 488(1941).

2. Wojtek J. Bock, Andrzel W. Komanski, and T. R.. Wolinski, *Applied Optics,* Vol. 29, No. 24, August 20, 1990.

3. Keithley MetraByte Corporation, "User Guide for the DAS-20," 1991.

4. H.M. Xio, P.Dabkiewicz, R. Ulrich, K. Okamoto, "Side Hole Fiber for Fiber Optic Pressure Sensing," *Opt. Lett.,* Vol. 11, No. 5, P.333, 1986.

5. K. Jansen, P. Dabkiewicz, "High Pressure Fiber-Optic Sensor with Side Hole Fiber," *Proc. SPIE.* Vol. 798, P.56, 1987.

6. P.S. Theocaris, E.E. Gdoutos, *Matrix Theory of Photoelasticity*, New York, Springer-Verlag Berlin Heidelberg, Chapters 3, 4, 6 and 7, 1979.

7. New Port Corporation, "Projects in Fiber Optics," 1986.

8. Shi-Kay Yao and Charles K. Asawa, "Fiber Optical Intensity Sensors," *IEEE Journal on Selected Areas in Communications,* Vol. SAC-1, No. 3, April 1983.

9. Grant R. Fowles, *Introduction to Modern Optics*, New York, Holt, Rinehart and Winston Inc., 1968.

10. Transportation Research Board, *Use of Weigh-in-Motion Systems for Data Collection and Enforcement,* National Research Council, National Cooperative Highway Research Program Synthesis of Highway Practice 124, 1988.

11. Ashish M. Vengsarkar, W. Craig Michhie, Ljilja Jankovic, Brian Culshaw, and Richard O. Claus, "Fiber Optic Sensor for Simultaneous Measurement of Strain and Temperature," *SPIE-The International Society for Optical Engineering, fiber Optic and Laser Sensor,* VIII, P.249-260, 1990.

12. T.H. Chua and Chin-lin Chen, "Fiber Polarimetric Stress Sensors," *Applied Optics,* Vol. 28, No.15, August 1989.

13. Wei Ma, "Polarimetric Fiber Optic Sensor for the Measurement of Strain," *NJIT Master's Thesis,* 1991.

14. James W. Dally and William F. Riley, *Experimental Stress Analysis*, McGraw-Hill Book Company, 1978.

15. Al-Rashid, Nasser I., Lee, Clyde E., and Dawkins, William P., "A Theoretical and Experimental Study of Dynamic Highway Loading," *Research Report No. 1081F Austin: Center of Highway Research, The University of Texas at Austin,* 1972.

16. Basson, J.E.B., and Slavik, M.M. "An Accuracy Study of the Axle Weight Analyser," *NITTR Report RP/3/75,* National Institute for Transport and Road Research, Pretoria, South Africa, 1975.

17. Basson, J.E.B. "The Effective Measurement of Traffic Axle Loading to Achieve Better Road Design," *NITRR Report RP/1/82. National Institute for Transport and Road Research,* 1981.

18. Salter, D.R., Davies, P. And Bettison, M, "The Development of Detector for the Measurement of Moving Wheel Loads," *14th Annual UTSTG* Conference, University of Leeds, United Kingdom, 1981.

19. Fregger, S. "Collection and use of Truck Characteristics Data," *Proceedings of the National Weigh in Motion Conference.* Denver, Colorado, July 1983.

20. "Weigh-in-Motion," RTAP Final Report, RTAP-WIM-8351(001), Arizona Department of Transportation, Phoenix, Arizona, 1985.

21. Basson, J.E.B., and Patterson, W.D.O. "A Brief Description of the NITRR," *Technical Note TP/5/79*, National Institute for Transport and Road Research, Pretoria, South Africa, 1979.

22. Basson, J.E.B., "The Installation of the Axle Weight Analyser," *NITRR Technical Note TP/5/79*, National Institute for Transport and Road Research, Pretoria, South Africa, 1979.

23. Electromatic (Pty) Ltd., *Traffic Axle Weight Classifier*, South Africa, Publicity leaflet. Electromatic (Pty) Ltd., Peitermaritzburg, (not dated).

24. Freeme, C.R., "The Development and Evaluation of a Porrtable Axle Weight Analyser," *NIRR Report RB/2/1972*, South Africa National Institute for Road Research, Pretoria, South Africa, 1972.

25. Copeland, K., "State Experience with WIM Systems-Streeter Amet System," *Proceedings of the National Weigh-in-Motion Conference*, Denver, Colorado, 1983.

26. Shouldel, L., "Weigh-in-Motion in Illinois," *Proceedings of the Second National Conference on Weigh-in-Motion Technology and Applications*, Atlanta, Georgia, 1985.

27. Sodern, *A Piezo-Electric Analysis of Road Traffic*, France, Laying Handbook for the Vibracoax Sodern Suresnes, (not dated).

28. Sodern, *VIBRACOAX-Detector for Traffic Analysis including In-Motion Axle Weight Classifications*, France, Product information brochure, Sodern, Suresnes, (not dated).

29. Cete de l'Est. *Cashier des Charges Provisior sur les Capteurs PiesoElectriques.* Cete de l'Est. Dept. Exploitation, Securite, Circulation. Groupe metrologie, Automatism., Paris, France, 1979.

30. TRRL, *Eastern CETE Tests and Tests at the Trappes Regional Laboratory (Paris West).* TRRL Translation, No. 2820, (not dated).

31. Siffert, M., "L'Exploitation des Bascules Dynamiques," *Bulletin de liaison des Laboratoires Ponts et Chaussees*, No. 70, March-April, P.814, 1974.

32. Gloagan, M. And M. Herbeuval, "Detection of Road Traffic by a Piezo-Electric Transducer," LEEA, Nancy, France, (not dated).

33. Bergeron. R., and Robert, M. "High Speed Sorter and Data Collection WIM System Highway 20, St. Romuald Province of Quebec, Canada," *Proceedings of the Second National Conference on Weigh-in-Motion Technology and Applications.* Atlanta, Georgia, May 1985.

34. Luc B. Jeunhomme. *Single-Mode Fiber Optics, Principle and Application*, New York and Basel, Marcel Dekker Inc., 1983.